5-3-2018 2:45 PM

Hydrogen Generation from Eosin Y-sensitized Pt/ZnO under Solar Light Irradiation

Tianfang Tian
The University of Western Ontario

Supervisor
Ray, Ajay K.
The University of Western Ontario

Graduate Program in Chemical and Biochemical Engineering
A thesis submitted in partial fulfillment of the requirements for the degree in Master of Science

Abstract

Hydrogen is a promising alternative energy carrier. Generating hydrogen via photocatalysts is clean and energy saving comparing to the current technology for hydrogen generation.

ZnO has been proved to have photocatalytic activities for wastewater treatment by multiple studies. However, there are not enough studies to investigate its potential to generate hydrogen as the photocatalyst under light irradiation. Therefore, we will investigate the photocatalytic ability of Pt/ZnO to generate hydrogen. Triethanolamine (TEOA) was used as sacrificial reagent while Eosin Y was used as sensitizer.

Pt/ZnO was characterized and tested for its activity for hydrogen generation in different conditions, which are platinum loading, pH value, EY to catalyst mass ratio, photocatalyst loading, TEOA concentration and light intensity.

The results showed that 0.75w% Pt/ZnO exhibited highest activity with hydrogen generation rate of 6.504 μmol min^{-1} under solar light irradiation.

Keywords

Photocatalysis, metal loading, hydrogen generation, solar, co-catalyst, platinum.

Acknowledgments

First, I would like to give my sincere gratitude to my supervisor Prof. Ajay K. Ray for his kind instruction, sincere help and understanding. Whenever I have confusion, he will always be willing be guide me with enormous patience and intelligence.

I would also like to thank my parents for their unconditional supports so that I could always face the difficulties with a big and strong heart. Their love provides me with warmth and safety that accompany me to study and live in a different country.

My colleagues Malini, Manoli, Daria and Mrinmoyee were always so helpful when I was working for my subject. They never hesitate to give me their hands whenever I need help and supports. Thank you for all the help and instructions all these years.

I would also express my sincere gratitude to technical stuff: Pastor Solano-Flores, Ying Zhang and Venkateswara Reddy Kandlakuti for giving me technical supports through my research.

Finally, thank you my dear friends. Thank you for your company and the happiness that you brought to me during my staying. Without you, I would never make it.

I feel so blessed to have all the supports, help and love with me through all these years!

Table of Contents

List of Figures

Nomenclature

C_0	initial concentration (g l^{-1})
Dye*	excited state of dye
Dye^+	oxidized form of dye
e^-	electron
EY	eosin Y
ΔG	Gibbs free energy
h^+	excited hole
h	plank's constant
k	reaction rate constant
K	absorption constant
λ	wavelength of light (nm)
ν	frequency (s^{-1})
μmol	micromole
TEOA	triethanolamine

Dedication

To my dear parents and friends

Love you all

Chapter 1

1 Introduction

1.1 Background and motivation

Global warming caused by greenhouse gases (GHGs) is a huge problem that we are facing right now. Efficient scientific evidence has accumulated to prove its exisitence. CO_2 and methane are reported to be two main resources of Green house gases (GHGs).[1–4] According to the recorded data, the contents of CO_2 are having a persistent increase with the average increase rate of 1.7 ppm yr^{-1} (from 1980 to 2011), mostly in the Northern Hemisphere.[5] Moreover, mole fraction of CH_4 has increased more than two times since 1750. Globally averaged CH_4 in 1750 was approximately 722 ppb but in 2011, the global annual mean has reached 1803 ppb.[5] The combustion of fossil oil and land use change are believed to be two main resources for the increase of CO_2 and CH_4.[5–7]

One of the most obvious consequences of global warming is temperature rising, leading to the rise of sea level and decline of glaciers and permafrost area.[8,9] If we only consider extra CO_2 and methane released from permafrost area, the estimated loss would reach $43 billion.[10] The loss caused by global warming is tremendous each year and has an increasing tendency along with the aggravation of global warming.[11] The growing release of GHGs would not only result in temperature rising but also result in changes in extreme events which would cause even more negative impact on environment and human society, such as inland flooding and hurricane.[12,13]

To deal with this problem, finding a clean, renewable and sustainable alternative new energy is essential for industry. Looking back to human history of fuels, the industrial energy has developed from wood to coal to oil to nowadays natural gas, the ratio of hydrogen to carbon has increased from 1:3-1:10 (wood) to 1:2 (coal) to 2:1 (oil) and now to 4:1 (natural gas).[14,15] In other words, fuels are going through the process of “decarbonization”. “Decarbonization” can not only effectively relieve the climate changes cause by GHGs emission, but also improve the utilization efficiencies of fuel energy.[16] Therefore, hydrogen is expected to be the future promising energy resources.[17–

[19] However, the difficulties of applying hydrogen as new energy lie in designing proper production approach and building sustainable energy system.[20,21] Although hydrogen is the most abundant and vastly distributed element on Earth, and accounts for 75% of universe mass, hydrogen exists only in combination forms with other elements on Earth and need to be seperated for its industrial use.[22]

Based on the technology that we have right now, the most commonly used one to generate hydrogen is by fuel processing.[23] Among the three primary techniques of fuel processing which is steam reforming, partial oxidation and auto-thermal reforming, steam reforming of methane is the most extensively applied technique.[23] Although steaming reforming technique has advantages of the absence of oxygen, low reaction temperature and high H_2/CO ratio, the sulfur that contained in methane will deactivate catalyst gradually and steaming reforming also has the highest emission among the three techniques which is harmful to environment.[23–26] Therefore, it is necessary to find a new technology to produce hydrogen which is both efficient and environmental friendly.

Generating hydrogen from photocatalysis using solar irradiation is an attractive option that has drawn massive attention in recent years because it is both clean, energy saving and renewable, shown in eq. (1.1). If we succeed in producing hydrogen by splitting water with the efficiency that high enough for commercial use, the emission of GHGs can then be greatly decreased so that global warming could be contained in this way.

$$\mathrm{H_2O} \xrightarrow{h\nu} \mathrm{H_2} + \frac{1}{2}\mathrm{O_2} \qquad \Delta G = +238\,\mathrm{kJ/mol} \tag{1.1}$$

However, the main barrier for the application of photocatalysis for hydrogen generation is its low efficiency. Overall water splitting with solely solar irradiation is the ultimate goal, but most of the photocatalyst can only be active under ultraviolet region of light. However, ultraviolet region only consists of 4% of solar light energy, resulting in the waste of majority of light energy. Although there are a few photocatalysts that have been reported to be active under visible light irradiation, such as GaN: ZnO,[27] the efficiency is still too low for it to be used commercially for it requires photocatalyst to have a proper

band gap and appropriate band positions. Therefore, sacrificial reagent system has been vastly used to increase hydrogen production efficiency.[28]

Compared to TiO_2 which has been the mostly investigated photocatalysts for its ability to split water, research about the ability of zinc oxide for hydrogen generation has been quite limited. Most of the research has been focusing on the photocatalytic degradation ability of zinc oxide for wastewater treatment instead of for hydrogen generation.[29–31] Comparing to TiO_2, ZnO is cheaper and easier to access, but ZnO has disadvantages of slightly larger band gap (3.3 eV)[32] which is slightly bigger than that of TiO_2 (3.2 eV), and it also has photo-corrosion problem which dramatically decreases its efficiency and stability. Noble metal loaded ZnO can realize efficient separation of excited electrons and holes to reduce the happening of the recombination reaction such as Ag,[33,34] Pt,[35,36] and Au,[37,38] usually have low overpotential for hydrogen evolution reaction (HER) which attracts electrons to migrate to noble metal sites while holes remain on the surface of photocatalysts.[39] Therefore, the photocatalytic performances and stability of photocatalysts can be enhanced.

1.2 Thesis objective & structure

Since the concept of photocatalyst to split water was brought up in 1972, thousands of papers have been published, but studies on the potential of dye-sensitized ZnO to split water is very limited. A brief review of studies about the hydrogen production potential was listed below.

Since the concept of photocatalyst to split water was brought up in 1972, thousands of papers have been published, but studies on the potential of dye-sensitized ZnO to split water is very limited. A brief review of studies about the hydrogen production potential was listed below:

Photocatalysts	**Light source**	**Sacrificial reagent**	**H_2 generation rate (μmol l^{-1})**	**Author**
ZnO/ TiO_2	visible	methanol	1.44	*Guo et al.*[40]

(core/shell)				
ZnO/CdS (nanoparticle)	visible	Na_2S/Na_2SO_3	3.00	*Wang et al.*[41]
Pt-ZnO-CdS@Cd (shell)	visible	Na_2S/Na_2SO_3	320	*Wang et al.*[42]
Ru-complex-Pt/ZnO	visible	/	1.12	*Dhanalakshmi et al.*[43]
CuO/ZnO (corn-like)	UV	methanol	2.83	*Liu et al.*[44]
ZnO/Pt/CdS (core-shell)	visible	Na_2S/Na_2SO_3	18.7	*Lingampalli et al.*[45]
ZnO/Pt/$Cd_{1-x}Zn_xS$ (x=0.2)	visible	Na_2S/Na_2SO_3	20.8	*Lingampalli et al.*[45]
CdS/ZnO/CdO	visible	Na_2S/Na_2SO_3	0.019	*Navarro et al.*[46]

The objective of this paper is to make up for the blank in the area of the photocatalytic performances of EY-sensitized Pt loaded ZnO for hydrogen generation. The specific parameters that were tested were:

- Loading content of Pt onto ZnO
- pH value of slurry
- Solar and visible light intensity
- TEOA solution concentration

- EY to Pt/ZnO weight ratio
- Photocatalyst loading

The structure of thesis is as following: i) Chapter 1 is about the background of my research topic, ii) Chapter 2 is about the review of the research topic, iii) Chapter 3 is about the experimental section of this thesis. iv) Chapter 4 is the conclusions and recommendations of further studies.

1.3 References:

1. Ehhalt, D. *et al.* Atmospheric Chemistry and Greenhouse Gases. (2001).

2. Houghton, R. A., Hackler, J. L. & Lawrence, K. T. The U.S. Carbon budget: contributions from land-Use change. *Science* **285,** 574–8 (1999).

3. Kiehl, J. T. & Trenberth, K. E. Earth ' s Annual Global Mean Energy Budget. 197–208

4. Rodhe, H. A comparison of the contribution of various gases to the greenhouse effect. *Science* **248,** 1217–9 (1990).

5. Dentener, F. J. *et al.* Observations: Atmosphere and Surface.

6. Searchinger, T. *et al.* Use of U.S. croplands for biofuels increases greenhouse gases through emissions from land-use change. *Science* **319,** 1238–40 (2008).

7. Fearnside, P. M. Global Warming and Tropical Land-Use Change: Greenhouse Gas Emissions from Biomass Burning, Decomposition and Soils in Forest Conversion, Shifting Cultivation and Secondary Vegetation. *Clim. Change* **46,** 115–158 (2000).

8. Stendel, M. & Christensen, J. H. Impact of global warming on permafrost conditions in a coupled GCM. *Geophys. Res. Lett.* **29,** 1632 (2002).

9. Hughes, L. Biological consequences of global warming: is the signal already apparent? *Trends Ecol. Evol.* **15,** 56–61 (2000).

10. Hope, C. & Schaefer, K. Economic impacts of carbon dioxide and methane released from thawing permafrost. **6,** (2016).

11. Cox, P. M., Betts, R. A., Jones, C. D. & Spall, S. A. Acceleration of global warming due to carbon-cycle feedbacks in a coupled climate model. **408,** 184–187 (2000).

12. Dai, A. Drought under global warming: a review. *Wiley Interdiscip. Rev. Clim. Chang.* **2,** 45–65 (2011).

13. Van Aalst, M. K. The impacts of climate change on the risk of natural disasters. *Disasters* **30,** 5–18 (2006).

14. Olah, G. A. Beyond Oil and Gas: The Methanol Economy. *Angew. Chemie Int. Ed.* **44,** 2636–2639 (2005).

15. Dunn, S. Hydrogen futures : toward a sustainable energy system. **27,** 235–264 (2002).

16. Lozza, G. & Chiesa, P. Natural Gas Decarbonization to Reduce CO_2 Emission From Combined Cycles: Part A — Partial Oxidation. in *Volume 2: Coal, Biomass and Alternative Fuels; Combustion and Fuels; Oil and Gas Applications; Cycle Innovations* V002T04A014 (ASME, 2000). doi:10.1115/2000-GT-0163

17. Züttel, A., Borgschulte, A., Schlapbach, L. (Louis) & Wiley InterScience (Online service). *Hydrogen as a future energy carrier*. (Wiley-VCH, 2008).

18. Züttel, A., Remhof, A., Borgschulte, A. & Friedrichs, O. Hydrogen: the future energy carrier. *Philos. Trans. A. Math. Phys. Eng. Sci.* **368,** 3329–42 (2010).

19. Edwards, P. P., Kuznetsov, V. L., David, W. I. F. & Brandon, N. P. Hydrogen and fuel cells: Towards a sustainable energy future. *Energy Policy* **36,** 4356–4362 (2008).

20. Turner, J. A. Sustainable hydrogen production. *Science* **305,** 972–4 (2004).

21. Elam, C. C. *et al.* Realizing the hydrogen future: the International Energy Agency's efforts to advance hydrogen energy technologies. *Int. J. Hydrogen Energy* **28,** 601–607 (2003).

22. Momirlan, M. & Veziroglu, T. N. The properties of hydrogen as fuel tomorrow in sustainable energy system for a cleaner planet. **30,** 795–802 (2005).

23. Holladay, J. D., Hu, J., King, D. L. & Wang, Y. An overview of hydrogen production technologies. **139,** 244–260 (2009).

24. Xu, J. & Froment, G. F. Methane steam reforming, methanation and water-gas shift: I. Intrinsic kinetics. *AIChE J.* **35,** 88–96 (1989).

25. Rostrup-Nielsen, J. R. Catalytic Steam Reforming. in *Catalysis* 1–117 (Springer Berlin Heidelberg, 1984). doi:10.1007/978-3-642-93247-2_1

26. Haryanto, A., Fernando, S., Murali, N. & Adhikari, S. Current Status of Hydrogen Production Techniques by Steam Reforming of Ethanol: A Review. *Energy & Fuels* **19,** 2098–2106 (2005).

27. Maeda, K. *et al.* GaN:ZnO solid solution as a photocatalyst for visible-light-driven overall water splitting. *J. Am. Chem. Soc.* **127,** 8286–8287 (2005).

28. Reza Gholipour, M., Dinh, C.-T., Béland, F. & Do, T.-O. Nanocomposite heterojunctions as sunlight-driven photocatalysts for hydrogen production from water splitting. *Nanoscale* **7,** 8187–8208 (2015).

29. Shen, W. *et al.* Photocatalytic degradation for methylene blue using zinc oxide prepared by codeposition and sol – gel methods. **152,** 172–175 (2008).

30. Pardeshi, S. K. & Patil, A. B. A simple route for photocatalytic degradation of phenol in aqueous zinc oxide suspension using solar energy. **82,** 700–705 (2008).

31. Sheela, T., Nayaka, Y. A., Viswanatha, R., Basavanna, S. & Venkatesha, T. G. Kinetics and thermodynamics studies on the adsorption of Zn(II), Cd(II) and Hg(II) from aqueous solution using zinc oxide nanoparticles. *Powder Technol.* **217,** 163–170 (2012).

32. Srikant, V. & Clarke, D. R. On the optical band gap of zinc oxide. **5447,** (2005).

33. Liu, Y., Wei, S. & Gao, W. Ag/ZnO heterostructures and their photocatalytic activity under visible light: Effect of reducing medium. *J. Hazard. Mater.* **287,** 59–

68 (2015).

34. Gao, P., Ng, K., materials, D. S.-J. of hazardous & 2013, undefined. Sulfonated graphene oxide–ZnO–Ag photocatalyst for fast photodegradation and disinfection under visible light. *Elsevier*

35. Yu, C. *et al.* Novel hollow Pt-ZnO nanocomposite microspheres with hierarchical structure and enhanced photocatalytic activity and stability. *Nanoscale* **5,** 2142 (2013).

36. Wenderich, K. & Mul, G. Methods, Mechanism, and Applications of Photodeposition in Photocatalysis: A Review. *Chem. Rev.* **116,** 14587–14619 (2016).

37. Naknam, P., … A. L. journal of & 2009, undefined. Preferential CO oxidation over Au/ZnO and Au/ZnO–Fe2O3 catalysts prepared by photodeposition. *Elsevier*

38. Wu, J., Environmental, C. T.-A. C. B. & 2006, undefined. Photocatalytic properties of nc-Au/ZnO nanorod composites. *Elsevier*

39. Yu, C. & Kai, Y. Novel hollow Pt-ZnO nanocomposite microposheres with hierarchical structure and enhanced photocatalytic activity and stability. 2142–2151 (2013). doi:10.1039/c2nr33595f

40. Wang, M. *et al.* Dye-sensitized solar cells based on nanoparticle-decorated ZnO/TiO $_2$ core/shell nanorod arrays. *J. Phys. D. Appl. Phys.* **42,** 155104 (2009).

41. Wang, X. *et al.* Enhanced photocatalytic hydrogen evolution by prolonging the lifetime of carriers in ZnO/CdS heterostructures. *Chem. Commun.* **0,** 3452 (2009).

42. Wang, X. *et al.* ZnO-CdS@Cd Heterostructure for Effective Photocatalytic Hydrogen Generation. *Adv. Energy Mater.* **2,** 42–46 (2012).

43. Dhanalakshmi, K. ., Latha, S., Anandan, S. & Maruthamuthu, P. Dye sensitized hydrogen evolution from water. *Int. J. Hydrogen Energy* **26,** 669–674 (2001).

44. Liu, Z., Bai, H., Xu, S. & Sun, D. D. Hierarchical CuO/ZnO ‘corn-like’ architecture for photocatalytic hydrogen generation. *Int. J. Hydrogen Energy* **36,** 13473–13480 (2011).

45. Lingampalli, S. R., Gautam, U. K. & Rao, C. N. R. Highly efficient photocatalytic hydrogen generation by solution-processed ZnO/Pt/CdS, ZnO/Pt/Cd1−xZnxS and ZnO/Pt/CdS1−xSex hybrid nanostructures. *Energy Environ. Sci.* **6,** 3589 (2013).

46. Navarro, R. M., Sánchez-Sánchez, M. C., Alvarez-Galvan, M. C., Valle, F. del & Fierro, J. L. G. Hydrogen production from renewable sources: biomass and photocatalytic opportunities. *Energy Environ. Sci.* **2,** 35–54 (2009).

Chapter 2

2 Review

Hydrogen is a promising alternative energy sources in the future. Splitting water via photocatalysts under solar irradiation is a potential way to produce hydrogen for commercial use. Photocatalysts are types of semiconductors, such as TiO_2,[1–7] ZnO,[8–14] CdS,[15–20] Ta_2O_5 [21,22] and ZrO_2,[23,24] that have conduction band and valence band, which can produce excited electrons and holes when irradiated by light with proper wavelength.[25,26] The excited electrons and holes can move from the bulk of semiconductor to the surface and react with water molecules to split water for generating hydrogen or degrading wastewater.

Numerous semiconductors have been tested for their photocatalytic activities to produce hydrogen since TiO_2 was first investigated for its photocatalytic ability to split water under UV light irradiation in 1972 by Fujishima and Honda.[27] However, although many semiconductors have been proved for their photocatalytic activities under UV light irradiation, the limited spectrum responsive area and low efficiencies have hindered the application of photocatalysts. Therefore, a vast amount of studies on photocatalysts modification have been conducted to improve the efficiencies of the photocatalyst to reach the commercial standard, such as co-catalyst loading,[28–31] doping,[32–35] and dye sensitization.[1,36–39] Besides, sacrificial agent system and Z-scheme system have also been tested for their contributions to photocatalytic performances. However, up to now, no photocatalyst has been reported to have the efficiencies that are high enough to split water for commercial use.

The difficulties of finding the efficient photocatalysts are the strict requirements for the band gap and the band positions of photocatalysts, the fast recombination rate of the excited holes and electrons inside the bulk of semiconductor as well as the stability of photocatalysts against photo-corrosion. Therefore, although overall water splitting is the ultimate goal, it has been barely realized by now. Although there are a few photocatalysts that are able to initiate whole water splitting, such as GaN:ZnO[9] and Cu_2O[40], but their

efficiencies are still too low for commercial application by far. Therein, more studies should be proceeded to further investigate the mechanism and modification of photocatalysts to improve the efficiency and stability of photocatalysts to larger extent.

This review will introduce the topic in following aspects, the basic principle of water splitting and basic properties of photocatalysts, challenges of water splitting via photocatalysts, sacrificial agent system as well as Z-scheme system in photocatalysis, different modification methods that can be applied to improve the efficiencies of photocatalysts which are co-catalyst loading, doping, nano-material hybridization and dye sensitization, and the corresponding methodologies to achieve the above modifications.

2.1 Basic principles of water splitting via semiconductor

2.1.1 Properties of semiconductors

Semiconductors are a type of materials that the electrical conductivity of which lie between conductors.[41] This property is special compared to metal and other materials. Semiconductor in bulk size have conduction band and valence band and the energy level difference between them is called band gap.[42,43] The value of band gap reveals the smallest energy required for electrons absorbed from light photons to be excited from valence band to vacant conduction band while leaving holes in valence band as shown in Fig. 1.[42,44] The excited electrons and holes can then mobilize in the influence of external electric field and can recombine with each other while emit energy in the form of heat or photons. Because of the special structures of semiconductors, certain sort of semiconductors particles can split water under light irradiation to produce hydrogen if certain requirements can be satisfied which will be discussed in detail in the following section.

Thermodynamically, water splitting reaction is an uphill reaction for its Gibbs energy value is unfavorably positive (+237 kJ mol^{-1}) which not only means that external energy need to be provided but also implies the backward reaction could happen easily. To initiate the water splitting reaction, the position of conduction band of semiconductor need to be lower than the reduction potential of hydrogen evolution reaction (HER) that

reduce H^+ to H_2 molecules while the position of valence band of semiconductor should be higher than the oxidation potential of oxygen evolution reaction (OER) that oxidize H_2O to O_2.[45,46] In other words, the band gaps of the semiconductors should be larger than the overpotential of the water splitting reaction which is 1.23 eV to achieve the water splitting reaction.[47] Moreover, considering the energy loss caused by entropy change and kinetic loss of excited electrons and holes migration and recombination, the minimum band gap energy of semiconductor need to be larger than the theoretical value of 1.23 eV [22]. Although the above requirement is not hard to meet for many semiconductors (Fig. 2), such as TiO_2, ZnO, and ZnS, only a few semiconductors can initiate water splitting reaction in visible light section while most of them can only be activated under UV light irradiation, such as $NaTaO_3$,[48] $La_2Ti_2O_7$,[49] and Sr_2Nb_2O.[50] The reasons of the above phenomenon will be discussed below.

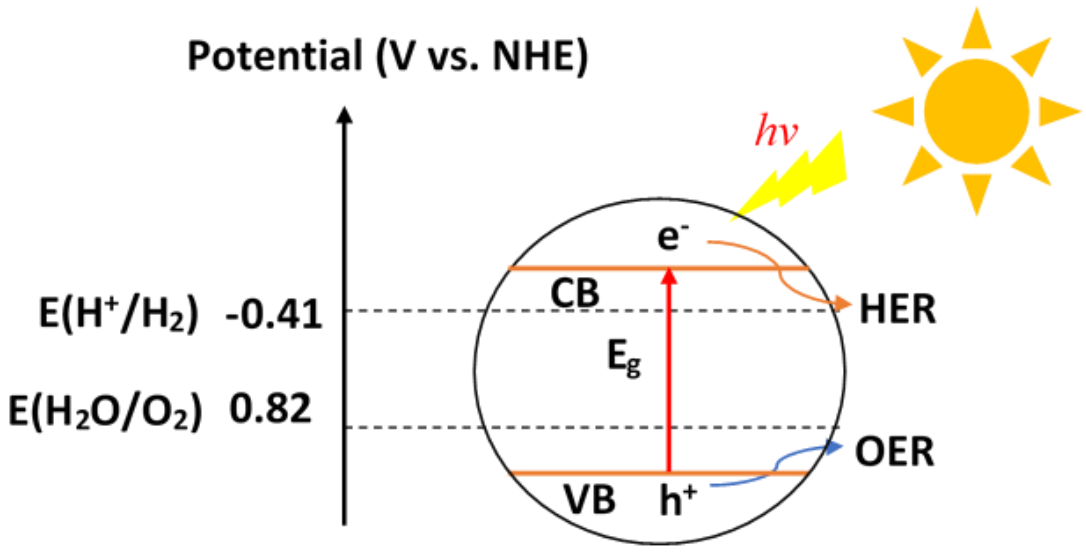

Figure 2. 1 Principles of water splitting via semiconductors

Large band gap greatly hinders the utilization of solar energy because it requires more energy to for semiconductors to be activated. As mentioned before, excited electrons need to overcome the band gap (E_g) between conduction band and valence band to complete the transition while leaving corresponding holes (h^+) in valence band. Therefore, the larger the band gap of semiconductor, the shorter the wavelength of light can be utilized by electrons to complete the transition. However, UV light section (λ<400

nm) only accounts for less than 5% of light energy while visible light section accounts for 46% of light energy, so large band gap will cause massive energy loss on light absorption. The relation between band gap and light wavelength can be expressed by $E_g = 1240/\lambda$, (where Eg is the band gap and λ is the maximum wavelength of light that can be absorbed) so based on this equation, to utilize the visible light (λ> 400 nm) energy, the band gap of semiconductors cannot be larger than 3.1eV, and considering the loss of energy transfer from incident light photons to the electrons of semiconductors, the band gap must be smaller than the calculated value above.

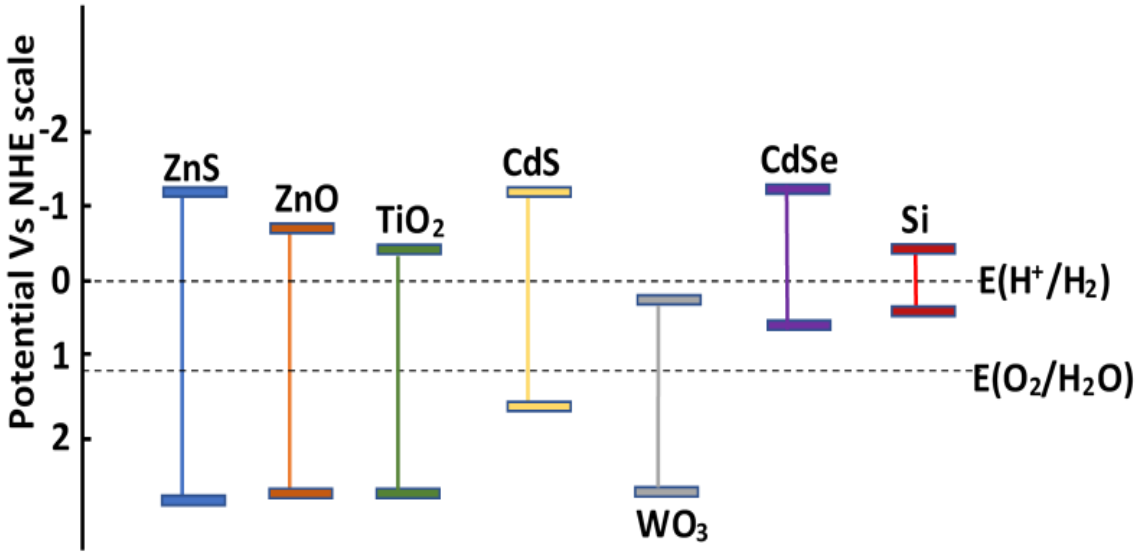

Figure 2. 2 Band gap potential of semiconductors

Besides the strict requirements for the positions of conduction band and valence band as well as value of band gap, the recombination rate of excited electrons and holes happens really fast which also limits the application of photocatalysts. For example, the recombination rate in bulk of TiO_2 happens in order of nanosecond. The above phenomenon can be attributed to the excited electron-hole recombination is in competitive relation with happening of HER and OER determined by the procedure of water splitting process. The procedure of overall water splitting process can be mainly described in 4 steps: (i) semiconductors absorb light energy and excited electrons was produced and transit from valence band to conduction band while leaving holes in

valence band, (ii) the excited holes and electrons migrate to the surface of the semiconductors, (iii) the excited holes and electrons recombine with each other inside the bulk of semiconductors, (iv) the excited electrons and holes on the surface of semiconductors react with H_2O molecules to generate hydrogen and oxygen. The recombination of excited electrons and holes is also called the backward reaction because it can be regarded as the reverse reaction of the production and separation of excited electrons and holes. Therefore, if the recombination of excited holes and electrons happens too fast inside the bulk of photocatalysts, they won't have time to move to the surface of semiconductors to participate HER and OER, leading to the low efficiency of photocatalysts. The competitive relation of step (ii) and (iii) makes the separation of electrons crucial for the water splitting reaction. Therein, to increase the rate of water splitting reaction, separation of electrons and holes need to be enhanced to hinder the backward reaction while promoting water splitting reaction.

Stability of semiconductors is very important to photocatalysts for it closely relates with crucial factors like wavelength response and photocatalytic activities. Metals are most popular elements for semiconductors for their characteristics in electronic and optical states. However, they usually have the tendency to go through photo-corrosion when they are in exposure of aqueous solution and under light illumination. The occurrence of photo-corrosion greatly decreases the stability of semiconductors for their anions are easier to be oxidized than H_2O molecules, such as CdS, ZnO and TaOH.[22,51,52] The mechanism of photo-corrosion of different semiconductors varies with their crystallinity and their chemical composites but normally it related to defects of semiconductors. For example, the mechanism of photo-corrosion of ZnO is mainly about the escaping of oxygen atoms via reacting with trapped photo-induced holes along with the fast expulsion of Zn^{2+} which mostly happens in structural defects on the surface of ZnO as shown below.[53–55]

$$O^{2-}_{surface} + h^{+} = O^{-}_{surface} \tag{2.1}$$

$$O^{-}_{surface} + 3O^{2-} + 3h^{+} = 2(O - O^{2-}) \tag{2.2}$$

$$O - O^{2-} + 2h^{+} = O_2 \quad (2.3)$$

$$2Zn^{2+} \rightarrow 2Zn_{aq}^{2+} \quad (2.4)$$

Therefore, an energy barrier should be built to hinder the happening of photo-corrosion such as coupling with stable semiconductors or noble metal, and doping metal elements that have higher resistance to corrosion. Methods that can be applied to solve the above problem will be discussed below.

Therefore, an energy barrier should be built in order to hinder the happening of photo-corrosion such as coupling with stable semiconductors or noble metal, and doping metal elements that have higher resistance to corrosion. Methods that can be applied to solve the above problem will be discussed below.

2.1.2 Sacrificial reagent systems

As mentioned before, efficient excited electron-hole pairs separation is crucial for the improvement of photocatalytic performances. The introduction of sacrificial agent system (one photon system) can effectively address the above problem by conducting only half of the water splitting reaction instead of the overall water splitting reaction. The principle of sacrificial agents is to sacrifice themselves to react with one type of charge carrier (e^- /h^+) so that the other type of charge carrier could have more opportunities to migrate to the surface of the semiconductors and react with H_2O to produce hydrogen or oxygen so that the utilization of one type of charge carrier can be remarkably increased, as shown in Fig. 4.[56] Generally, sacrificial agents can be categorized in two types which are the electron donors and electron acceptors. Electron donors, which called hole scavenger, refer to the sacrificial agents that consume excited holes, leaving excited electrons to participate HER. When OER is excluded, the value of ΔG can be dramatically decreased, lowering the energy barrier. Typical examples of organic (hydrocarbon) hole scavengers are triethanolamine (TEOA), ethylenediaminetetraacetic acid (EDTA), methanol, ethanol and glycerol. The most representative inorganic hole scavenger is Na_2S-Na_2SO_3 which have been tested and proved to be capable of enhancing the photocatalytic activities and stability.[57] Among photocatalysts, SO_3^{2-}/S^{2-} is the most common used sacrificial agent for

metal sulfides, especially for CdS, for it can effectively address the problem of photo-corrosion which is common in metal-sulfide photocatalysts. The above phenomenon can be attributed to the dissolving of photo-corrosion reaction product S to SO_3^{2-}/S^{2-} solution which can remarkably decrease the deposition of S to CdS.[47] Electron acceptors refer to the sacrificial agents that react with excited electrons, leaving excited holes to participate OER. Typical examples of electron acceptors are Fe^{3+},[58] and Ce^{4+},[58] which can be easily reduced by photo-induced electrons to Fe^{2+}, Ce^{3+}.

To select the proper sacrificial agent, the redox potential of sacrificial agents should be firstly considered. For hole scavenger, the oxidation potential of hole scavenger should be lower than oxidation potential of OER which means hole scavenger is more readily oxidized by photo-induced holes in valence band on the surface of semiconductors than water molecules. It has been reported that the higher the redox potential, the faster hole scavenging is, which can effectively enhance the quantum efficiency and stability.[59] Melián et al.[60] conducted a study of the effect of different organic sacrificial agents on hydrogen production when Pt modified TiO_2 was used as photocatalyst. The result showed that the effectiveness of sacrificial agents decreasing in the sequence of methane > ethanol > ethylene glycol > glycol. Nada et al.[6] also tested the effect of different organic sacrificial agents on hydrogen production, using modified TiO_2 as photocatalyst and the result of which showed that the ranking of them was following the sequence of EDTA > methanol > ethanol > lactic acid.

Although photocatalysts that need sacrificial agent seems useless, they can still be used in Z-scheme system and have great potential in biomass.[61,62]

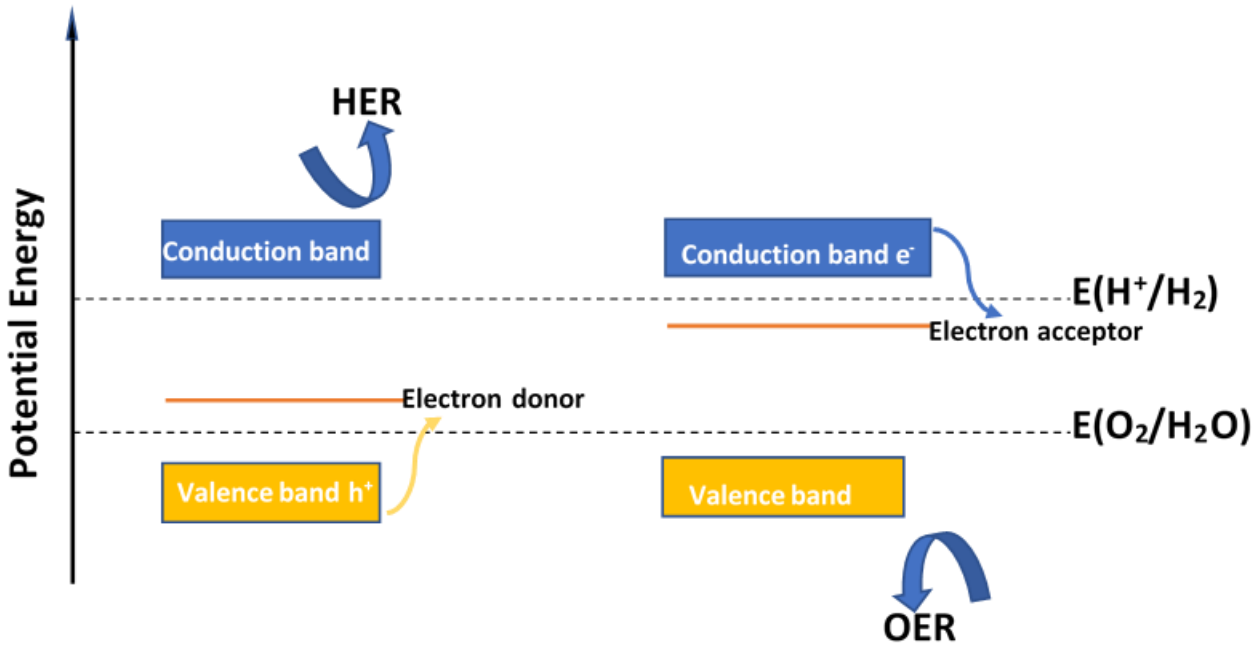

Figure 2. 3 Schematic of the principles of water reduction or oxidation in sacrificial agent system

2.1.3 Z-scheme system

Z-scheme system is inspired by natural photosynthesis of green plants, which can also be called electron mediator system. The principle of this system is to split overall water splitting into two steps by using two different electron mediators which will return to their original chemical states after reacting with excited electrons or holes as shown in Fig. 5 .[56] As explained before, splitting overall water splitting into HER and OER will become thermodynamically favorable for the value of ΔG will decreases a lot and the utilization of photons can be enhanced in this way. Therefore, semiconductors with improper band gaps and band positions can still acts as photocatalysts in Z-scheme system and therein Z-scheme system can enlarge the selecting range of semiconductors. Moreover, the separation of HER and OER can lead to the effective separation of excited electrons and holes and therein the backward reaction can be suppressed. The most extensively used electron mediators are Fe^{3+}/Fe^{2+},[29] Ce^{4+}/Ce^{3+},[63] and $IO3^{-}/I^{-}$.[64,65]

The drawbacks of Z-scheme system compared to sacrificial agent system is the number of photons needed to trigger the reaction is larger than that of one photon system since

extra photons are needed for OER. Besides, Z-scheme system is relatively more complicated so that the selectivity of chemical reactions that can occur during water splitting reaction should also be considered.

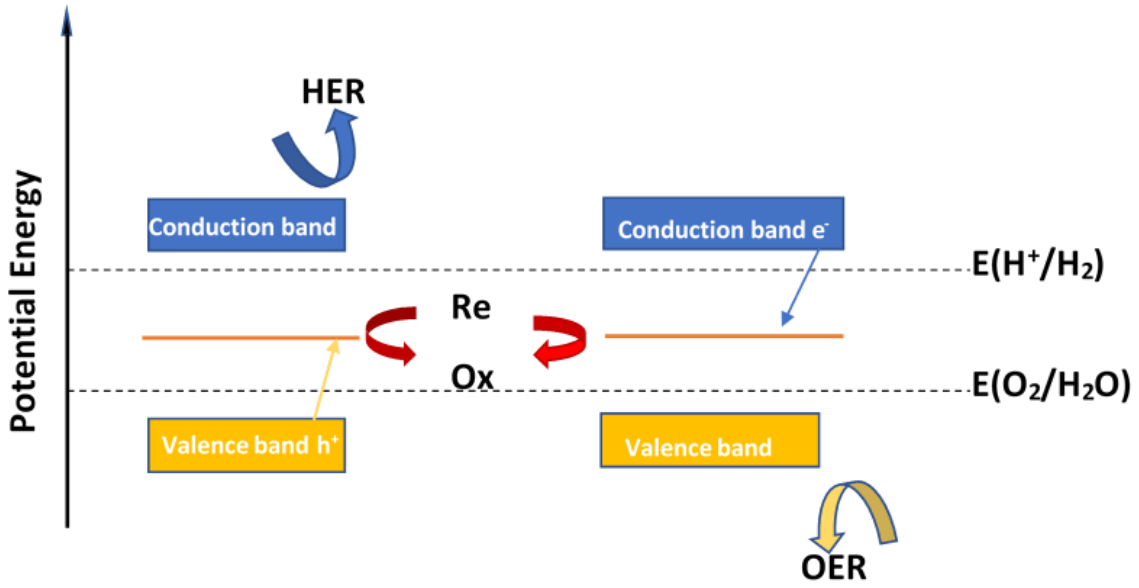

Figure 2. 4 Schematic of the principles of overall water splitting in the Z-scheme system[56]

2.2 Photocatalyst modification

As the requirements of semiconductors to split water are very strict, most semiconductors cannot conduct overall water splitting without modification in high hydrogen generation rate. Therefore, photocatalyst modification has drawn massive attention since the concept of photocatalyst was first brought up. As mentioned before, there are mainly four steps in the process of water splitting via semiconductors. Photocatalyst modification can influence step (i) by narrowing the band gap of semiconductors (band engineering) to enhance the absorption of light energy, separating electron-hole pairs to water splitting reaction improvement (step (ii) and step (iii)), adjusting band positions of semiconductors to fit the energy level required by water splitting reaction (step (iv)), and stabilizing semiconductors to expand the lifetime of the semiconductors.

2.2.1 Metal deposition

Transition metals are usually chosen to be co-catalysts for semiconductors because they have multiple oxidation states and easily lose the electrons because transition metals have these properties, they are often chosen as co-catalyst for semiconductors. Among them, noble metals are most extensively used to be loaded onto semiconductors to enhance their photocatalytic performances for the reason that Fermi energy level is low in noble metals compared to semiconductors, so noble metals can act as strong magnets or trappers to attract excited electrons from semiconductors to co-catalyst sites while leaving holes inside the bulk of surface or migrating to the surface of the semiconductors, which is also called Schotty barrier as a sort of junction that gives rise to charge separation as shown in Fig. 2.3.[56,66] Therefore, it can effectively separate excited electrons and holes so that the recombination of excited electrons and holes can be hindered. When the backward reaction is suppressed, water splitting reaction will be promoted. In other words, the loading of co-catalysts can provide active reduction sites for water splitting reaction for the overpotential of HER in noble metals is much smaller than that of semiconductors. Noble metals, such as Pt,[30,67–70] Au,[71–76] and Ag,[31,77–82] have been tested and proved to have the abilities to improve the photocatalytic activities of semiconductors remarkably. Especially Pt, based on the research carried out by Trasatti[83] about the relation of exchange current of HER on metal and the work function, the absorption heat of hydrogen to Pt is about 16 kcal mol^{-1} which is lowest among all the metals, most favorable for the occurrence of HER. The particle size, loading content and morphology of loaded noble metal oxide can cause huge differences to their effect on the photocatalytic activities of semiconductors with noble metal loading. Besides, it has been reported that the loading of noble metal can also suppress photo-corrosion while remarkably increase the stability of some semiconductors, such as Pt/ZnO,[84] and Pt/CdS.[69]

However, the overloading of metal compounds can result in the decrease of photocatalytic activities because of the formation of recombination center, the decrease of light absorption active sites area and the increase of light scattering. Therefore, finding the optimal condition for metal loading is very important for its application.

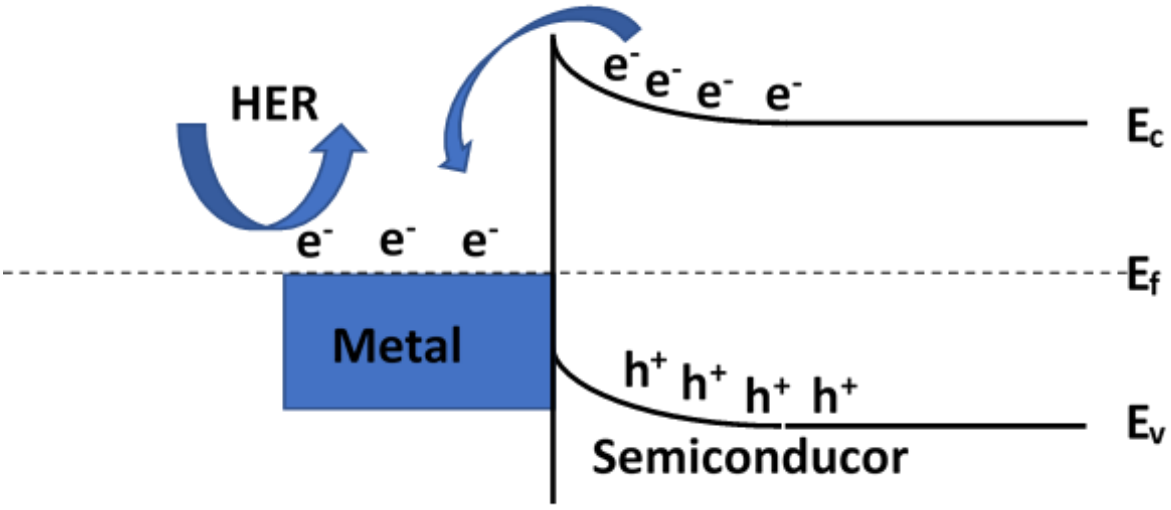

Figure 2. 5 Schematic of the energy band model of a Schottky junction (E_f represents fermi energy level, E_c and E_v represent conduction band energy level and valence band energy level)

2.2.2 Binary composites coupling

Metal oxides, metal sulfides, metal nitrides, metal oxynitrides and metal oxysulfides have been coupled with different semiconductors and increase the photocatalytic activities of semiconductors. WO_3 is a typical example of binary composites in metal oxides. WO_3 itself is a type of semiconductor but it doesn't have photocatalytic activities for water splitting, the reason of which can mainly be concluded as the CB position of WO_3 is lower than the oxygen reduction potential of OER. However, if couple WO_3 with other semiconductor like TiO_2, the hydrogen generation rate can be increased greatly. The principle of the above phenomenon is that adequate amount of WO_3 coupling increases the surface area of the photocatalyst and the formation of chemical bond of W-O-Ti can effective separate the excited electron-hole pairs to reduce the backward reaction as the positions of their valence band and conduction band helps the excited electrons to migrate from TiO_2 to WO_3.[85–87]

CdS is a representative example in metal sulfides and has been coupled to semiconductors like ZnO, TiO_2 to enhance the water spitting activities. Metal sulfides

like CdS (2.4 eV) usually have narrow band gap which is in favor of light absorption and can act as photosensitizers. Therefore, coupling CdS to semiconductors can assist light energy harvesting and excited electrons and holes production. Increased surface to volume ratio via CdS coupling can also provide more active sites for photocatalytic reaction as well as promote vectorial transfer from host photocatalyst to CdS, favorable to electron-hole separation. Although CdS is unstable when independently used as photocatalyst, coupling CdS to photocatalysts with high stability like TiO_2,[88] SnO_2[89] can greatly improve the stability of the coupling semiconductor.[16] It has been tested and proved that CdS/TiO_2 can be used for both wastewater treatment and hydrogen generation. Moreover, CdS/TiO_2 can produce hydrogen in visible light irradiation for the maximum wavelength of photons absorbed is 520 nm.[88] The coupling of CdS and TiO_2 has higher hydrogen generation rate than both TiO_2 and CdS when used separately. Beside the reasons that mentioned above, the prominent photocatalytic performances shown by CdS/TiO_2 can be explained by the relative positions of conduction band and valence band, which can be categorized as one type of heterojunction as shown in Fig 2.4. In this situation, the valence band of semiconductor 1 (TiO_2) is higher than the coupling semiconductor 2 (CdS) so that excited electrons can migrate from semiconductor 2 to 1 driven by potential difference while photo-induced holes can migrate from semiconductor 1 to 2 through heterojunctions. The principles of the above type of heterojunctions can remarkably enhance the separation between two types of carriers. Besides the above materials, CdSe,[4] SiO_2,[90] Al_2O_3,[91] ZrO_2,[92] SnO_2,[93] and CuO[94] have also been proved to have the ability to improve the photocatalytic performances of semiconductors.

Oxynitride and oxysulfides with metal cations in d^0 and d^{10} electronic configuration have been tested and proved to have the capability to split water under light illumination. Among oxynitride with d^0 electronic configuration, TaON have the highest apparent quantum yield and has been reported to be photoresponsive for overall water splitting under visible light illumination after loaded with metal or binary composites, such as Pt or Ta_3N_5.[95,96] For the type of photocatalysts of d^{10} electronic configuration, it was first reported by Sato et al.[97] in 2005 that Ga_3N_4 coupled with RuO_2 can be photoresponsive in UV light illumination for water splitting because the band gap of β-Ga_3N_4 is as large as

3.8 eV. Domen et al. also reported in 2005 that solid solution of gallium and zinc nitrogen oxide, which can be expressed as $(Ga_{1-x}Zn_x)(N_{1-x}O_x)$, modified with RuO_2 and Cr_2O_3 can split water under visible light irradiation.[98] Compared to d^{10} electronic configuration, d^0 electronic configuration has wider spectra absorption, leading to higher light utilization.[99,100] Most of oxynitride with d^0 electronic configuration have absorption bands at 500 – 750 nm, so they are usually active under visible light irradiation for water splitting with presence of sacrificial agents.

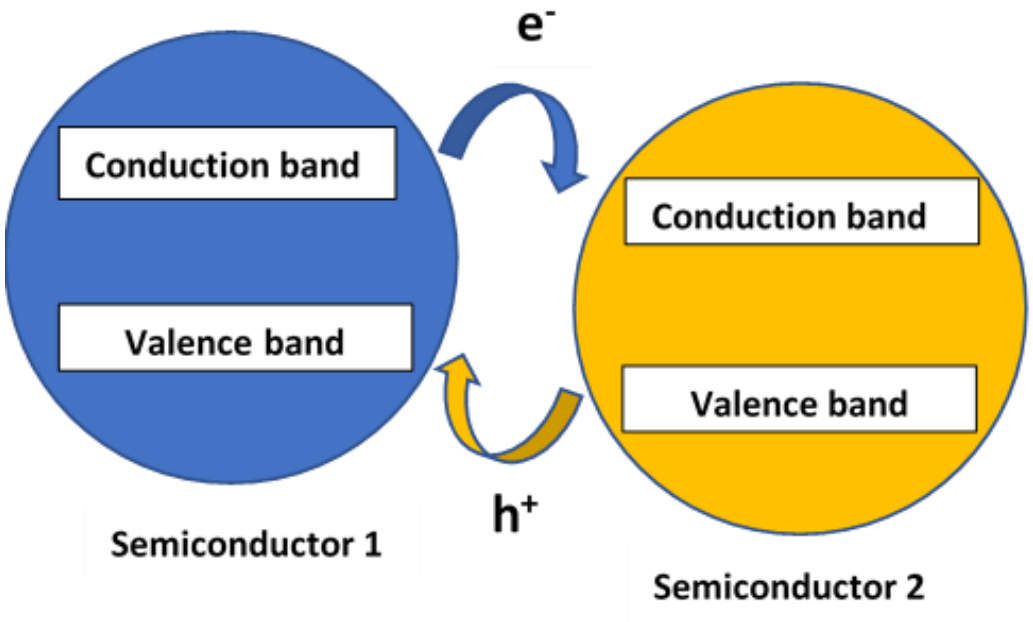

Figure 2. 6 One typical type of heterojunction structure of semiconductors

In conclusion, the binary composites coupling can increase the photocatalytic performances of semiconductors by increasing specific surface, reducing electron-hole recombination and enhancing the light absorption. However, optimal point of coupling should be investigated in each case for overloading can also result in decreasing of photocatalytic activities for the formation of recombination center.

2.2.3 Doping

Doping can be seen as defect engineering.[22] Like materials choosing of co-catalyst, transition metal and noble metal ions (cation ions) are often used for metal doping, such

as Fe,[8] Sb,[101] Mn,[102] and Cr.[103] Although these two methods share the similar range of materials that can be chosen, their principles are totally different from each other. Unlike co-catalyst loading, doping is to introduce defects to semiconductor which aims to trap excited electrons and holes and therein to effectively separate the excited electrons and holes and inhibit backward reaction. Doping can make two major changes to semiconductors: (i) adjusting the positions of energy levels of transition metals that used for doping locate between the band gaps of semiconductors, creating intermediate states in between and can be called defect states. Therefore, the shortening of distance from the positions of valence band (at the bottom) to defect states (at the middle) and from defect states (at the middle) to conduction band (at the top) makes the transition of excited electrons or holes easier to occur under longer wavelength of light, (ii) directly shifting the positions of conduction band and valence band to narrow down the band gap of semiconductors.[22] For example, Pt doped TiO_2 is promisingly active under visible light irradiation which can be attributed to the existence of Pt redox energy via Pt ion doping that shortens the band gap of semiconductor so that the efficiency of solar energy utilization is improved.[104]

Besides transitional metal, nonmetallic material (anion ions) have also been studied as dopants, such as Carbon,[105] sulfur,[106] and boron.[107] However, although it has been reported by some studies that it can increase the photocatalytic activities of certain semiconductors, compared to metal ion doping, nonmetallic ion doping is more controversial because some contradictory cases have been reported. The above phenomenon may be ascribed to the formation of recombination center for vacancies caused by the introduction of dopants, resulting in the destruction of crystallinity.

Co-doping with hetero-ions has synergistic effect on photocatalytic performances of semiconductors. Metal-metal doping (Zn^{2+}/Fe^{3+},[108] Sb/Cr),[109] nonmetal-nonmetal doping (Br/Cl,[110] N/S)[111] and metal-nonmetal doping (La^{3+}/N,[112] Fe^{3+}/N,[113] graphene/Fe^{3+})[114] have all been investigated on their effect to photocatalytic activities. In principle, co-doping can deepen the doping length and content. Therefore, the dispersion and uniformity of distribution could be improved. However, the studies of co-doping on different substrate showed contradictory results. For example, although it has been

proved that co-doping can enhance the degradation of methyl blue (MB),[115] there is no study shows the improvement of degradation of phenol via co-doping of TiO_2 compared to single doping so far. Therefore, the effect of co-doping may vary according to the substrate and model molecules that are used.

Therefore, more studies should be conducted to investigate the reaction mechanism of nonmetallic material doped semiconductors.

2.2.4 Carbon nano-material hybridization

Carbon Nano-material such as carbon nanotube,[116,117] graphene,[118] C_{60} (water soluble),[53] and C_3N_4[119] has been investigated for their potential to increase photocatalytic activities of semiconductors remarkably. The above phenomenon can be ascribed to physical and photo-chemical properties of carbon-nanomaterials. This kind of materials have large specific surface area and sufficient π-bond with surface electric charge. For example, carbon nanotube hybridization, especially multi-walled carbon nanotubes (MWCNT) hybridization has been proved to be effective to increase specific area, electron-hole separation and enhance light absorption of photocatalysts such as ZnO, TiO_2 and Pt. The introduction of MWCNT with oxygen-containing groups, such as hydroxyl, carbonyl, and carboxylic functionalities, to the system helps to promote electronic transfer at long wavelength light irradiation, improving production of excited electrons and holes. Moreover, the relative band edge positions of MWCNT of host photocatalysts allows excited electrons to transfer from semiconductors to conducting network of carbon nanotube, inhibiting recombination of electrons and hole. The large specific area of carbon-nanotube can assist semiconductors to absorb degradation model or dyes to enhance the photocatalytic performances of semiconductors. Moreover, it was reported that C_{60} can remarkably inhibit the photo-corrosion of ZnO for vacancies that can react with excited holes, resulting in oxygen escape will act as anchoring site for C_{60} so that the unsaturated bond of oxygen atoms won't be easily triggered and therein photo-corrosion can be hindered by this way.[53] The main limitations of using carbon nano-material lie in the solubility and difficulties of manipulation in solvent. Therefore, more studies need to be carried out to investigate the mechanism further.

2.2.5 Dye-sensitized of photocatalysts

As mentioned before, most of semiconductors cannot be photoresponsive under visible light irradiation for improper band gaps, such as WO_3, TiO_2 and ZnO. Dye-sensitization is one of the most effective and simple method to widen the responsive spectra range while also increases the efficiency of the excitation process. Up to now, organic dyes (metal-free dyes), and metal complexes are the two main kinds of dyes that are most extensively used and studied in the field of photocatalysis. Metal-free dyes, such as Eosin Y,[38,120–122] Rhodamine-B (RhB),[123–125] cyanine,[126,127] and riboflavin,[128–130] have prominent photochemical properties like large molar absorption coefficient and high quantum yield.[126,131] Moreover, metal-free dyes, because of their hydrocarbon composites, are easy to design and prepare according to different requirements.

Coordination metal complexes, such as ruthenium-based catalysts,[116,132–134] and porphyrin-based catalysts,[135–138] have advantages of regenerative sensitization, widened spectrum responsive area and enhanced photocatalytic performances, which have drawn massive attention in related field. The main drawback of metal complexes sensitization is the difficulties of stable dye anchoring caused by large molecule size. The anchoring of dyes is dependent on the crystallinity of the host catalysts which means the natural properties of different photocatalysts and synthesis methods can both play important roles in dye anchoring process.

Mechanism of dye sensitization can be briefly expressed by following equations:

$$\mathrm{Dye} + h\nu \rightarrow \mathrm{Dye}^{*} \tag{6}$$

$$\mathrm{Dye}^{*} + \mathrm{A} \rightarrow \mathrm{Dye}^{+} + \mathrm{A}^{-} \tag{7}$$

The first step of dye sensitization is the excitation of dye molecules as shown in eq. (6). During this step, electrons transit from the highest occupied molecular orbital (HOMO) to the lowest occupied molecular orbital (LUMO) of the dye molecules that have absorbed onto the surface of semiconductors.[139] Although some dyes have the capability to emit electrons without the presence of semiconductors, absence of electron/hole separator (semiconductors) greatly prohibits the happening of HER or OER. The

following step is the electron injection from LUMO of dye molecules to the conduction band of semiconductors, which happens in order of femtosecond depending on the nature of dyes while recombination reaction happens in order of nanoseconds to miliseconds inside the bulk of semiconductors.[36,140,141] One example was shown in Fig 2.7 about the schematic diagram of possible reaction routes of dye-sensitized TiO_2.[142] Serpone et al.[143] have reported that most of the photo-induced electron-hole recombination reactions happen in ~10 ns. Fast electron injection and slow backward reaction can efficiently separate electrons and holes, leading to blockage of the recombination reaction. The excited electrons then quickly move to the surface of semiconductors which enables electrons to produce hydrogen or degrade pollutants. Moreover, when semiconductors are modified with metals, such as Pt and Au, dye molecules can attach themselves to metal loaded sites with a much stronger chemical bond than that of between dyes and semiconductors, developing an energy band between the band gap to greatly enhance the photocatalytic performances.[38] Although instability of dye molecules will largely decrease the photocatalytic activities of the system along with the ongoing of photocatalytic reactions, the existence of sacrificial agents, such as Fe^{3+}/Fe^{2+} and EDTA, can effectively address the above problem because sacrificial agents, as electron donors, can give electrons back to excited dye molecules to regenerate dye molecules, prolonging the lifetime of dye molecules.

The sensitization of photocatalysts by organic dyes and metal complexes has been applied to different aspects, which are visible-light-induced photo-degradation of various contaminants, dye-sensitized solar cells (DSSC), and the photocatalytic hydrogen generation under visible light irradiation. Based on studies, the photocatalytic activities and efficiencies of sensitized photocatalysts applied to different fields have all been tested and proved to be improved via low cost and convenient fabrication methods.

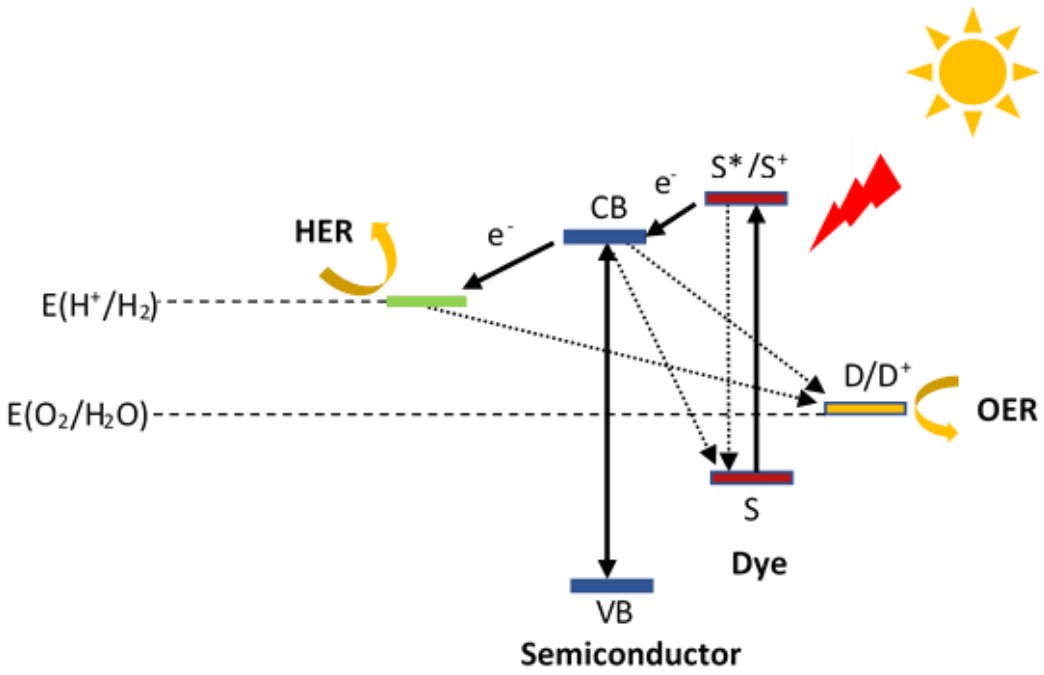

Figure 2. 7 Schematic diagram of dye-sensitized photocatalysts under light illumination[142] and possible backward reaction pathway (dotted line)

2.3 Methods of photocatalyst modification

2.3.1 Photo-deposition

Photo-deposition method is to deposit metal or metal oxide nanoparticles on the surface of semiconductors by utilizing the solar light illumination in an aqueous phase with presence of metal precursors and usually with presence of sacrificial agents.[144] Photo-deposition was first successfully conducted in 1965 for the deposition of Ag to TiO_2 in slurry of $AgNO_3$ and TiO_2.[145] The first successful deposition of Pt to TiO_2 was in 1978 and since then this method has drawn huge attention in photocatalysis and have been applied to the modification of a vast range of semiconductors, such as TiO_2,[144,146–149] ZnO,[79,84,144,150–152] WO_3,[71,86,144,153,154] CdS,[17,144,155,156] and $SrTiO_3$.[29,157–160] The successful loading of metals to semiconductors via photo-deposition depends on the happening of reductive reaction of metal ions (aqueous phase) to metal (solid phase) while the loading of metal oxides depends on the occurrence of oxidative reaction of metal ions (aqueous phase) to metal oxides (solid phase).

To make photo-deposition happen, there are three main premises that need to be satisfied. First, the positions of conduction band of host semiconductors must be higher (more negative) than the redox potential of metal salt in aqueous phase as precursor. Second, the energy of photo-induced photons emitted by solar light must exceed the band gap of the host semiconductor so that positively charged metal ions can combine with excited electrons or holes produced by the host semiconductors via light irradiation. Third, efficient excited hole-electron pair's separation and active reactive sites are necessary for the happening of deposition. Sacrificial agents and PH value can dramatically enhance the rate of deposition as well as change the morphology of semiconductors as reported by Liu et al..[152]

Compared with other methods, photo-deposition is a simple and efficient in situ way to form co-catalyst on the surface of semiconductors for there is no need for temperature control or external potential to be added to the system. A study conducted by Behnajady et al.[161] has investigated the difference of photocatalytic activities of Ag/TiO_2 prepared by photo-deposition and impregnation. The result showed that Ag/TiO_2 prepared by photo-deposition has higher photocatalytic activities with lower Ag loading content on degrading C.I. Acid Red 88 (AR88) compared to Ag/TiO2 prepared by impregnation.[161] The above phenomenon can be explained by the smaller loaded metallic particles formed by photo-deposition enhancing dispersion. Therefore, photo-deposition is a very extensively used method in photocatalysis.

2.3.2 Impregnation

Impregnation is another widely used approach for photocatalyst loading. As photo-deposition, impregnation also need precursors in aqueous solution in which semiconductor will be impregnated followed by solvent evaporation or filtering and drying. The solid will then be further calcined to reach its active form. Huge amount of studies about modification of semiconductors via impregnation have proved that it is a simple and effective approach to modify various semiconductors, especially for doping.[162–165] The concentration of precursor and calcination temperature both have strong effect on the particle size, morphology and photocatalytic activities of the final photocatalysts. According to the studies on effect of different calcination temperature,

high calcination temperature will tend to reduce the photocatalytic activities of photocatalysts for two main reasons: (i) the transformation of crystallinity, such as TiO_2 can change from anatase to rutile in high temperature, (ii) decrease of dispersion of loading element for high calcination temperature can lead to the formation of bulky metallic particles, (iii) oxidative state changes of loading or doping element for the valence value change of loading element can change the chemical bond formation.[161,166] It has been reported by Kohtani et al.[167] that Ag/ $BiVO_4$ prepared by impregnation with lower Ag loading had higher degradation rate on phenol compared with Ag/$BiVO_4$ prepared by photo-deposition, and the reason of which could be attributed to the formation of silver oxides (Ag_2O and/or AgO) in the process of impregnation for the fact that phenol had the tendency to be absorbed easier onto the surface of silver oxides. However, in the photo-deposition process no oxidized silver could be detected. Therefore, in certain conditions, impregnation presents more advantages than other alternative

2.3.3 Chemical reduction

The above two methods are simple to conduct but when it is necessary to precisely control the ratio of certain elements, chemical reduction is a more effective way to prepare photocatalysts considering the precise synthesis realization. As reported by Wang et al.,[168] TaON can be coupled with Ta_3N_5 via in situ chemical reduction method. In this method, $TaCl_5$ was dissolved in bromoethane as precursor and then was mixed with TaON followed by consistent stirring to recover it in the form of powder. The reactor was maintained at -45 ^oC with condensed ammonia gas in the form of sodium solution which was followed by the above powder adding. Byproduct was removed by condensed ammonia and then the mixture was heated at 800 ^oC to crystallize it under nitrogen atmosphere.

Another example was the synthesis of Ta particles by using $TaCl_5$, sodium and liquid ammonia. $TaCl_5$ and sodium were separately dissolved in liquid ammonia in two chambers and then mixed together for the reduction reaction to occur. The byproduct is NaCl and can be removed from the system by liquid ammonia followed by the final

product filtering. Similarly, Nb_3Al can be prepared by $AlCl_3$ and $NbCl_5$ reacting with sodium-ammonia following the above procedure.[169]

2.3.4 Electrodeposition

Electrodeposition method is an attractive method to prepare photocatalysts for low cost, moderate operating temperature, and easily controlled thickness of films. The photocatalytic performances of a vast range of semiconductors have been reported to increase by modification via electrodeposition, such as CuO,[170] TiO_2,[5,171,172] ZnO,[173] and Fe_2O_3.[174] For example, Ag/TiO_2 has been reported to be synthesized by electrodeposition method.[175] The starting step of this method is coating TiO_2 with a Si substrate followed by drying at 100 ^oC. Electrodeposition was conducted in a three-electrode cell with Ag/AgCl as reference electrode and Pt as counter electrodes with an electrolyte solution mixed by Ag (II) perchlorate hydrate and $NaClO_4$ by amperometry. Another example is the preparation of CuO/ZnO nanocomposite film.[173] Electrodeposition process was conducted at the current density of 3 mA cm^{-2} for 15 min on a pre-treated substrate coated by indium tin oxide (ITO) in the bath mixed by $Zn(NO_3)_2$ and $Cu(CHCOO)_2$ solution, and the concentration of which was determined by the ratio of Cu/Zn. The temperature of the above procedure was maintained at 65 ^oC.

2.3.5 Atomic-layer deposition

ALD is a layer-by-layer thin film growth technology which uses self-limiting surface reaction steps in the presence of precursors.[176] ALD method has advantages of controlling the thickness at atomic level and composition precisely, moderate reaction temperature, and realizing uniform growth with high specific surface area, especially on loading ultrathin or conformal films.[24,177] Therefore, this method has attracted massive attention and has been applied to many metal-oxide semiconductors, such as TiO_2,[177,178] Al_2O_3,[179] and ZnO.[180] Zhou et al.[177] has conducted a study which showed massive increase on photocatalytic performances of TiO_2 by loading Pt via ALD. In the above study, a fluidized bed reactor (FBR) was chosen as the reactor for the reaction. $MeCpPtMe_3$ was chosen as solid precursor at the fixed temperature of 80 ^oC which was carried by nitrogen gas to enter the reactor followed by O_2 feeding. 0.2g substrate TiO_2

was loaded in FBR and $MeCpPtMe_3$ and O_2 were fed into the reactor with flow velocity of 0.8 cm/s and the temperature of reaction ranged from 150 ^oC to 400 ^oC. Different Pt loading was altered by changing the ALD super cycle ratio.

Liu et al.[181] conducted a study on the effect of Pt loading on different carbon substrate via ALD. Similarly, in this study, $MeCpPtMe_3$ and O_2 were used as precursors which were carried by pure nitrogen gas, and were purged into the reactor loaded with different substrates with uniform growth temperature of 250 ^oC. The result showed that Pt deposition on semiconductors via ALD has high dispersion and controllable particle sizes which provides effective solution to conventional problems of photocatalyst synthesis.

2.4 Conclusions

In this review the principles and challenges of hydrogen generation via photocatalysts were discussed. Light energy loss caused by strict requirements for semiconductors and fast recombination rate of e^-/h^+ are two main challenges. Modification methods like dye sensitization, cocatalyst, doping and binary composites coupling can be used to deal with the above problems.

Different synthesis methods were also summarized and discussed. Synthesis method should be chosen according to the different needs of photocatalysts. Among them, photodeposition and impregnation are two of the most extensively methods for photocatalyst modification.

Although a huge amount of papers has been published, there are still some topics need to be explored. For example, most research has been focusing on potential of modified TiO_2 for hydrogen generation while not enough work has been done to investigate the possibilities of ZnO as host photocatalyst to generate hydrogen. Compared with TiO_2, ZnO has much higher carrier mobility which is important factor that contributes to the efficiency of hydrogen production. Therefore, this thesis aims to explore the potential of modified ZnO as photocatalysts to generate hydrogen.

2.5 References:

1. O'Regan, B. & Gratzel, M. A Low-Cost, High-Efficiency Solar-Cell Based on Dye-Sensitized Colloidal TiO_2 Films. *Nature* **353,** 737–740 (1991).

2. Irie, H., Watanabe, Y. & Hashimoto, K. Carbon-doped Anatase TiO_2 Powders as a Visible-light Sensitive Photocatalyst. *Chem. Lett.* **32,** 772–773 (2003).

3. Park, H., Park, Y., Kim, W. & Choi, W. Surface modification of TiO2photocatalyst for environmental applications. *J. Photochem. Photobiol. C Photochem. Rev.* **15,** 1–20 (2013).

4. Ho, W. & Yu, J. C. Sonochemical synthesis and visible light photocatalytic behavior of CdSe and CdSe/TiO2nanoparticles. *J. Mol. Catal. A Chem.* **247,** 268–274 (2006).

5. Liu, X. *et al.* Electrodeposition preparation of Ag nanoparticles loaded TiO2 nanotube arrays with enhanced photocatalytic performance. *Elsevier*

6. Nada, A. A., Barakat, M. H., Hamed, H. A., Mohamed, N. R. & Veziroglu, T. N. Studies on the photocatalytic hydrogen production using suspended modified TiO2photocatalysts. *Int. J. Hydrogen Energy* **30,** 687–691 (2005).

7. Pore, V., Rahtu, A., Leskelä, M., Deposition, M. R.-… V. & 2004, undefined. Atomic layer deposition of photocatalytic TiO2 thin films from titanium tetramethoxide and water. *Wiley Online Libr.*

8. Baek, S., Song, J. & Lim, S. Improvement of the optical properties of ZnO nanorods by Fe doping. *Phys. B Condens. Matter* **399,** 101–104 (2007).

9. Maeda, K. *et al.* GaN:ZnO solid solution as a photocatalyst for visible-light-driven overall water splitting. *J. Am. Chem. Soc.* **127,** 8286–8287 (2005).

10. Kayaci, F., Ozgit-Akgun, C., Donmez, I., Biyikli, N. & Uyar, T. Polymer–Inorganic Core–Shell Nanofibers by Electrospinning and Atomic Layer

Deposition: Flexible Nylon–ZnO Core–Shell Nanofiber Mats and Their Photocatalytic Activity. *ACS Appl. Mater. Interfaces* **4,** 6185–6194 (2012).

11. Giuseppe Marcì, † *et al.* Preparation Characterization and Photocatalytic Activity of Polycrystalline ZnO/TiO2 Systems. 1. Surface and Bulk Characterization. (2001). doi:10.1021/JP003172R

12. Pacholski, C., Kornowski, A., Chemie, H. W.-A. & 2004, undefined. Site-Specific Photodeposition of Silver on ZnO Nanorods. *Wiley Online Libr.*

13. Sakthivel, S. *et al.* Solar photocatalytic degradation of azo dye : comparison of photocatalytic efficiency of ZnO and TiO 2. **77,** 65–82 (2003).

14. Wang, Y., Shi, R., Lin, J. & Zhu, Y. Enhancement of photocurrent and photocatalytic activity of ZnO hybridized with graphite-like C3N4. *Energy Environ. Sci.* **4,** 2922 (2011).

15. Fujii, M., Nagasuna, K., Fujishima, M., Akita, T. & Tada, H. Photodeposition of CdS Quantum Dots on TiO_2 : Preparation, Characterization, and Reaction Mechanism. *J. Phys. Chem. C* **113,** 16711–16716 (2009).

16. Qian, S. *et al.* An enhanced CdS/TiO2 photocatalyst with high stability and activity: Effect of mesoporous substrate and bifunctional linking molecule. *J. Mater. Chem.* **21,** 4945 (2011).

17. Chen, X., Chen, W., Gao, H., … Y. Y.-A. C. B. & 2014, undefined. In situ photodeposition of NiOx on CdS for hydrogen production under visible light: enhanced activity by controlling solution environment. *Elsevier*

18. Dukovic, G., Merkle, M. G., Nelson, J. H., Hughes, S. M. & Alivisatos, A. P. Photodeposition of Pt on Colloidal CdS and CdSe/CdS Semiconductor Nanostructures. *Adv. Mater.* **20,** 4306–4311 (2008).

19. Xie, K. *et al.* Electrochemical construction of Z-scheme type CdS–Ag–TiO2 nanotube arrays with enhanced photocatalytic activity. *Elsevier*

20. Jing, D. & Guo, L. A novel method for the preparation of a highly stable and active CdS photocatalyst with a special surface nanostructure. *J. Phys. Chem. B* **110,** 11139–11145 (2006).

21. Sreethawong, T., Ngamsinlapasathian, S., Suzuki, Y. & Yoshikawa, S. Nanocrystalline mesoporous Ta2O5-based photocatalysts prepared by surfactant-assisted templating sol-gel process for photocatalytic H2evolution. *J. Mol. Catal. A Chem.* **235,** 1–11 (2005).

22. Pan, H. Principles on design and fabrication of nanomaterials as photocatalysts for water-splitting. *Renew. Sustain. Energy Rev.* **57,** 584–601 (2016).

23. Lo, C. C., Hung, C. H., Yuan, C. S. & Wu, J. F. Photoreduction of carbon dioxide with H2and H2O over TiO2and ZrO2in a circulated photocatalytic reactor. *Sol. Energy Mater. Sol. Cells* **91,** 1765–1774 (2007).

24. Johnson, R. W., Hultqvist, A. & Bent, S. F. A brief review of atomic layer deposition: From fundamentals to applications. *Mater. Today* **17,** 236–246 (2014).

25. Rothenberger, G., Fitzmaurice, D. & Grätzel, M. Spectroscopy of conduction band electrons in transparent metal oxide semiconductor films: Optical determination of the flatband potential of colloidal titanium dioxide films. *J. Phys. Chem.* **96,** 5983–5986 (1992).

26. Mills, A. & Le Hunte, S. An overview of semiconductor photocatalysis. *J. Photochem. Photobiol. A Chem.* **108,** 1–35 (1997).

27. Fujishima, A. & Honda, K. Electrochemical photolysis of water at a semiconductor electrode. *Nature* **238,** 37–38 (1972).

28. Bai, S., Wang, L., Chen, X., Du, J. & Xiong, Y. Chemically exfoliated metallic MoS2nanosheets: A promising supporting co-catalyst for enhancing the photocatalytic performance of TiO2nanocrystals. *Nano Res.* **8,** 175–183 (2014).

29. Sasaki, Y., Iwase, A., Kato, H. & Kudo, A. The effect of co-catalyst for Z-scheme

photocatalysis systems with an Fe3+/Fe2+ electron mediator on overall water splitting under visible light irradiation. *J. Catal.* **259,** 133–137 (2008).

30. Li, X. *et al.* Single-Atom Pt as Co-Catalyst for Enhanced Photocatalytic H2Evolution. *Adv. Mater.* **28,** 2427–2431 (2016).

31. Jiang, D., Chen, L., Xie, J. & Chen, M. Ag $_2$ S/g-C $_3$ N $_4$ composite photocatalysts for efficient Pt-free hydrogen production. The co-catalyst function of Ag/Ag $_2$ S formed by simultaneous photodeposition. *Dalt. Trans.* **43,** 4878–4885 (2014).

32. Ho, W., Yu, J. C., Lin, J., Yu, J. & Li, P. Preparation and photocatalytic behavior of MoS2 and WS 2 nanocluster sensitized TiO2. *Langmuir* **20,** 5865–5869 (2004).

33. Ohno, T., Mitsui, T. & Matsumura, M. Photocatalytic Activity of S-doped TiO2 Photocatalyst under Visible Light. *Chem. Lett.* **32,** 364–365 (2003).

34. Xu, A. W., Gao, Y. & Liu, H. Q. The preparation, characterization, and their photocatalytic activities of rare-earth-doped TiO2nanoparticles. *J. Catal.* **207,** 151–157 (2002).

35. Konta, R., Ishii, T., Kato, H. & Kudo, A. Photocatalytic Activities of Noble Metal Ion Doped SrTiO $_3$ under Visible Light Irradiation. *J. Phys. Chem. B* **108,** 8992–8995 (2004).

36. Yan, S. G. & Hupp, J. T. Semiconductor-Based Interfacial Electron-Transfer Reactivity: Decoupling Kinetics from pH-Dependent Band Energetics in a Dye-Sensitized Titanium Dioxide/Aqueous Solution System. *J. Phys. Chem.* **100,** 6867–6870 (1996).

37. Malekshoar, G. & Ray, A. K. In-situ grown molybdenum sul fi de on TiO 2 for dye-sensitized solar photocatalytic hydrogen generation. **152,** 35–44 (2016).

38. Jin, Z., Zhang, X., Lu, G. & Li, S. Improved quantum yield for photocatalytic hydrogen generation under visible light irradiation over eosin sensitized TiO2-Investigation of different noble metal loading. *J. Mol. Catal. A Chem.* **259,** 275–

280 (2006).

39. Chowdhury, P., Gomaa, H. & Ray, A. K. Chemosphere Sacrificial hydrogen generation from aqueous triethanolamine with Eosin Y-sensitized Pt / TiO 2 photocatalyst in UV , visible and solar light irradiation. **121,** 54–61 (2015).

40. Hara, M. *et al.* Cu 2 O as a photocatalyst for overall water splitting under visible light irradiation. *Chem. Commun.* **2,** 357–358 (1998).

41. Bawendi, M. The Quantum Mechanics Of Larger Semiconductor Clusters (. *Annu. Rev. Phys. Chem.* **41,** 477–496 (1990).

42. Brus, L. E. & Brus, L. E. The size dependence of the lowest excited electronic state Electron-electron and electron-hole interactions in small semiconductor crystallites : The size dependence of the lowest excited electronic state. **4403,** (1998).

43. Alivisatos, A. P. Perspectives on the physical chemistry of semiconductor nanocrystals. *J. Phys. Chem.* **100,** 13226–13239 (1996).

44. Li, X. *et al.* Engineering heterogeneous semiconductors for solar water splitting. *J. Mater. Chem. A* **3,** 2485–2534 (2015).

45. Hisatomi, T., Kubota, J. & Domen, K. Recent advances in semiconductors for photocatalytic and photoelectrochemical water splitting. *Chem. Soc. Rev.* **43,** 7520–7535 (2014).

46. Abe, R. Recent progress on photocatalytic and photoelectrochemical water splitting under visible light irradiation. *J. Photochem. Photobiol. C Photochem. Rev.* **11,** 179–209 (2010).

47. Ni, M., Leung, M. K. H., Leung, D. Y. C. & Sumathy, K. A review and recent developments in photocatalytic water-splitting using TiO2for hydrogen production. *Renew. Sustain. Energy Rev.* **11,** 401–425 (2007).

48. Lee, Y. *et al.* Hydrothermal Synthesis of Fine $NaTaO_3$ Powder as a Highly Efficient Photocatalyst for Overall Water Splitting. *Bull. Chem. Soc. Jpn.* **80,** 423–428 (2007).

49. Kim, J., Hwang, D. W., Bae, S. W., Kim, Y. G. & Lee, J. S. Effect of precursors on the morphology and the photocatalytic water-splitting activity of layered perovskite La2Ti2O7. *Korean J. Chem. Eng.* **18,** 941–947 (2001).

50. Kudo, A., Kato, H. & Nakagawa, S. Water Splitting into H_2 and O_2 on New $Sr_2M_2O_7$ (M = Nb and Ta) Photocatalysts with Layered Perovskite Structures: Factors Affecting the Photocatalytic Activity. *J. Phys. Chem. B* **104,** 571–575 (2000).

51. Ito, S., Thampi, K., Comte, P., … P. L.-C. & 2005, undefined. Highly active meso–microporous TaON photocatalyst driven by visible light. *pubs.rsc.org*

52. Smith, A. M. & Nie, S. Semiconductor Nanocrystals: Structure, Properties, and Band Gap Engineering. *Acc Chem Res.* **43,** 190–200 (2010).

53. Fu, H., Xu, T., Zhu, S. & Zhu, Y. Photocorrosion Inhibition and Enhancement of Photocatalytic Activity for ZnO via Hybridization with C_{60}. *Environ. Sci. Technol.* **42,** 8064–8069 (2008).

54. Rudd, A. L. & Breslin, C. B. Photo-induced dissolution of zinc in alkaline solutions. *Electrochim. Acta* **45,** 1571–1579 (2000).

55. Genscher, H. Electrochemical Behavior of Semiconductors under Illumination. *J. Electrochem. Soc.* **113,** 1174 (1966).

56. Reza Gholipour, M., Dinh, C.-T., Béland, F. & Do, T.-O. Nanocomposite heterojunctions as sunlight-driven photocatalysts for hydrogen production from water splitting. *Nanoscale* **7,** 8187–8208 (2015).

57. Chen, X., Shen, S., Guo, L. & Mao, S. S. Semiconductor-based photocatalytic hydrogen generation. *Chem. Rev.* **110,** 6503–6570 (2010).

58. Bamwenda, G. R., Uesigi, T., Abe, Y., Sayama, K. & Arakawa, H. The photocatalytic oxidation of water to O2 over pure CeO2, WO3, and TiO2 using Fe3+ and Ce4+ as electron acceptors. *Appl. Catal. A Gen.* **205,** 117–128 (2001).

59. Berr, M. J. *et al.* Hole scavenger redox potentials determine quantum efficiency and stability of Pt-decorated CdS nanorods for photocatalytic hydrogen generation. *Appl. Phys. Lett.* **100,** 223903 (2012).

60. Craciun, V., Elders, J., Gardeniers, J., Films, J. G.-T. S. & 1995, undefined. Growth of ZnO thin films on GaAs by pulsed laser deposition. *Elsevier*

61. Colmenares, J. C. & Luque, R. Heterogeneous photocatalytic nanomaterials: prospects and challenges in selective transformations of biomass-derived compounds. *Chem. Soc. Rev.* **43,** 765–778 (2014).

62. Navarro, R. M., Sánchez-Sánchez, M. C., Alvarez-Galvan, M. C., Valle, F. del & Fierro, J. L. G. Hydrogen production from renewable sources: biomass and photocatalytic opportunities. *Energy Environ. Sci.* **2,** 35–54 (2009).

63. Kozlova, E. A., Korobkina, T. P. & Vorontsov, A. V. Overall water splitting over Pt/TiO2 catalyst with Ce3+/Ce4+ shuttle charge transfer system. *Int. J. Hydrogen Energy* **34,** 138–146 (2009).

64. Abe, R., Higashi, M., ChemSusChem, K. D.- & 2011, undefined. Overall Water Splitting under Visible Light through a Two-Step Photoexcitation between TaON and WO3 in the Presence of an Iodate–Iodide Shuttle Redox Mediator. *Wiley Online Libr.*

65. Abe, R., Sayama, K., Domen, K. & Arakawa, H. A new type of water splitting system composed of two different TiO2 photocatalysts (anatase, rutile) and a IO3−/I− shuttle redox mediator. *Chem. Phys. Lett.* **344,** 339–344 (2001).

66. JINHUI YANG HONGXIAN HAN, AND CAN LI*, D. W. *et al.* Roles of Cocatalysts in Photocatalysis and Photoelectrocatalysis. *Acc. Chem. Res.* **46,** 1900–1909 (2012).

67. Yamakata, A., Ishibashi, T. & Onishi, H. Electron- and Hole-Capture Reactions on Pt/TiO $_2$ Photocatalyst Exposed to Methanol Vapor Studied with Time-Resolved Infrared Absorption Spectroscopy. *J. Phys. Chem. B* **106,** 9122–9125 (2002).

68. Min, S., Energy, G. L.-I. J. of H. & 2012, undefined. Dye-cosensitized graphene/Pt photocatalyst for high efficient visible light hydrogen evolution. *Elsevier*

69. Nosaka, Y., Yamaguchi, K., … A. K.-… of P. and & 1992, undefined. Colloidal CdS—Pt photocatalyst stabilized by pendant viologen polymer for photoinduced electron transfer and hydrogen evolution. *Elsevier*

70. Zhang, N., Fu, X., Chemistry, Y. X.-J. of M. & 2011, undefined. green approach to synthesize Pt@ CeO 2 nanocomposite with tunable core-shell and yolk-shell structure and its application as a visible light photocatalyst. *pubs.rsc.org*

71. Tanaka, A., … K. H.-J. of the A. & 2014, undefined. Visible-Light-Induced Hydrogen and Oxygen Formation over Pt/Au/WO3 Photocatalyst Utilizing Two Types of Photoabsorption Due to Surface Plasmon. *ACS Publ.*

72. Wu, J., Environmental, C. T.-A. C. B. & 2006, undefined. Photocatalytic properties of nc-Au/ZnO nanorod composites. *Elsevier*

73. Samanta, S., Martha, S., ChemCatChem, K. P.- & 2014, undefined. Facile Synthesis of Au/g-C3N4 Nanocomposites: An Inorganic/Organic Hybrid Plasmonic Photocatalyst with Enhanced Hydrogen Gas Evolution Under Visible-Light. *Wiley Online Libr.*

74. Li, H. *et al.* Mesoporous Au/TiO $_2$ Nanocomposites with Enhanced Photocatalytic Activity. *J. Am. Chem. Soc.* **129,** 4538–4539 (2007).

75. Tanaka, A., Hashimoto, K. & Kominami, H. Visible-Light-Induced Hydrogen and Oxygen Formation over Pt/Au/WO $_3$ Photocatalyst Utilizing Two Types of Photoabsorption Due to Surface Plasmon Resonance and Band-Gap Excitation. *J. Am. Chem. Soc.* **136,** 586–589 (2014).

76. Samanta, S., Martha, S. & Parida, K. Facile Synthesis of Au/g-C $_3$ N $_4$ Nanocomposites: An Inorganic/Organic Hybrid Plasmonic Photocatalyst with Enhanced Hydrogen Gas Evolution Under Visible-Light Irradiation. *ChemCatChem* n/a-n/a (2014). doi:10.1002/cctc.201300949

77. Gao, P., Ng, K., materials, D. S.-J. of hazardous & 2013, undefined. Sulfonated graphene oxide–ZnO–Ag photocatalyst for fast photodegradation and disinfection under visible light. *Elsevier*

78. Zhu, M., Chen, P. & Liu, M. Graphene Oxide Enwrapped Ag/AgX (X = Br, Cl) Nanocomposite as a Highly Efficient Visible-Light Plasmonic Photocatalyst. *ACS Nano* **5,** 4529–4536 (2011).

79. Georgekutty, R., Seery, M. K. & Pillai, S. C. A Highly Efficient Ag-ZnO Photocatalyst: Synthesis, Properties, and Mechanism. *J. Phys. Chem. C* **112,** 13563–13570 (2008).

80. Hu, C., Lan, Y., Qu, J., Hu, X. & Wang, A. Ag/AgBr/TiO $_2$ Visible Light Photocatalyst for Destruction of Azodyes and Bacteria. *J. Phys. Chem. B* **110,** 4066–4072 (2006).

81. Yu, J., Dai, G. & Huang, B. Fabrication and Characterization of Visible-Light-Driven Plasmonic Photocatalyst Ag/AgCl/TiO $_2$ Nanotube Arrays. *J. Phys. Chem. C* **113,** 16394–16401 (2009).

82. Wang, P. *et al.* Highly Efficient Visible-Light Plasmonic Photocatalyst Ag@AgBr. *Chem. - A Eur. J.* **15,** 1821–1824 (2009).

83. Trasatti, S. Work function, electronegativity, and electrochemical behaviour of metals. III. Electrolytic hydrogen evolution in acid solutions. *J. Electroanal. Chem.* **39,** 163–184 (1972).

84. Yu, C. *et al.* Novel hollow Pt-ZnO nanocomposite microspheres with hierarchical structure and enhanced photocatalytic activity and stability. *Nanoscale* **5,** 2142 (2013).

85. Papp, J., Soled, S., Dwight, K. & Wold, A. Surface Acidity and Photocatalytic Activity of TiO2, WO3/TiO2, and MoO3/TiO2 Photocatalysts. *Chem. Mater.* **6,** 496–500 (1994).

86. Tae Kwon, Y., Yong Song, K., In Lee, W., Jin Choi, G. & Rag Do, Y. Photocatalytic behavior of WO3-loaded TiO2 in an oxidation reaction. *J. Catal.* **191,** 192–199 (2000).

87. Ahmad, H., Kamarudin, S. K., Minggu, L. J. & Kassim, M. Hydrogen from photo-catalytic water splitting process: A review. *Renew. Sustain. Energy Rev.* **43,** 599–610 (2015).

88. So, W., Kim, K., Energy, S. M.-I. journal of hydrogen & 2004, undefined. Photo-production of hydrogen over the CdS–TiO2 nano-composite particulate films treated with TiCl4. *Elsevier*

89. Ghugal, S. G., Umare, S. S. & Sasikala, R. A stable, efficient and reusable CdS–SnO2 heterostructured photocatalyst for the mineralization of Acid Violet 7 dye. *Appl. Catal. A Gen.* **496,** 25–31 (2015).

90. Du, Q. *et al.* Immobilized palladium on surface-modified Fe3O4/SiO2 nanoparticles: as a magnetically separable and stable recyclable high-performance catalyst for Suzuki and Heck cross-coupling reactions. *Tetrahedron* **68,** 3577–3584 (2012).

91. Hisao Yoshida, *, Norimitsu Matsushita, Yuko Kato, and & Hattori, T. Synergistic Active Sites on SiO2−Al2O3−TiO2 Photocatalysts for Direct Methane Coupling. (2003). doi:10.1021/JP034458+

92. Fu, X., Clark, L. A., Yang, Q. & Anderson, M. A. Enhanced Photocatalytic Performance of Titania-Based Binary Metal Oxides: TiO_2 /SiO_2 and TiO_2 /ZrO_2. *Environ. Sci. Technol.* **30,** 647–653 (1996).

93. Vinodgopal, K. & Kamat, P. V. Enhanced Rates of Photocatalytic Degradation of an Azo Dye Using SnO2/TiO2 Coupled Semiconductor Thin Films. *Environ. Sci.*

Technol. **29,** 841–845 (1995).

94. XIA, H., ZHUANG, H., ZHANG, T. & XIAO, D. Photocatalytic degradation of Acid Blue 62 over CuO-SnO2 nanocomposite photocatalyst under simulated sunlight. *J. Environ. Sci.* **19,** 1141–1145 (2007).

95. Hara, M. *et al.* TaON and Ta3N5 as new visible light driven photocatalysts. *Catal. Today* **78,** 555–560 (2003).

96. Chen, S. *et al.* Efficient Visible-Light-Driven Z-Scheme Overall Water Splitting Using a $MgTa_2O_{6-x}N_y$/TaON Heterostructure Photocatalyst for H_2 Evolution. *Angew. Chemie* **127,** 8618–8621 (2015).

97. Junya Sato, † *et al.* RuO2-Loaded β-Ge3N4 as a Non-Oxide Photocatalyst for Overall Water Splitting. (2005). doi:10.1021/JA042973V

98. Maeda, K. *et al.* GaN:ZnO Solid Solution as a Photocatalyst for Visible-Light-Driven Overall Water Splitting. *J. Am. Chem. Soc.* **127,** 8286–8287 (2005).

99. Maeda, K. & Domen, K. ChemInform Abstract: Solid Solution of GaN and ZnO as a Stable Photocatalyst for Overall Water Splitting under Visible Light. *ChemInform* **41,** no-no (2010).

100. Xu, J., Pan, C., Takata, T. & Domen, K. Photocatalytic overall water splitting on the perovskite-type transition metal oxynitride $CaTaO_2N$ under visible light irradiation. *Chem. Commun.* **51,** 7191–7194 (2015).

101. Mandalapu, L. J., Xiu, F. X., Yang, Z., Zhao, D. T. & Liu, J. L. p-type behavior from Sb-doped ZnO heterojunction photodiodes. *Appl. Phys. Lett.* **88,** 112108 (2006).

102. Deng, Q. R., Xia, X. H., Guo, M. L., Gao, Y. & Shao, G. Mn-doped TiO2 nanopowders with remarkable visible light photocatalytic activity. *Mater. Lett.* **65,** 2051–2054 (2011).

103. Ghicov, A., Schmidt, B., Kunze, J. & Schmuki, P. Photoresponse in the visible range from Cr doped TiO2 nanotubes. *Chem. Phys. Lett.* **433,** 323–326 (2007).

104. Kim, S., Hwang, S. J. & Choi, W. Visible light active platinum-ion-doped TiO2 photocatalyst. *J. Phys. Chem. B* **109,** 24260–24267 (2005).

105. Tan, S. T. *et al.* p-type conduction in unintentional carbon-doped ZnO thin films. *Appl. Phys. Lett.* **91,** 72101 (2007).

106. Geng, B. Y. *et al.* Synthesis and optical properties of S-doped ZnO nanowires. *Appl. Phys. Lett.* **82,** 4791–4793 (2003).

107. Wenas, W. W., Yamada, A., Takahashi, K., Yoshino, M. & Konagai, M. Electrical and optical properties of boron-doped ZnO thin films for solar cells grown by metalorganic chemical vapor deposition. *J. Appl. Phys.* **70,** 7119–7123 (1991).

108. Yuan, Z., Jia, J. & Zhang, L. Influence of co-doping of Zn(II)+Fe(III) on the photocatalytic activity of TiO2 for phenol degradation. *Mater. Chem. Phys.* **73,** 323–326 (2002).

109. Valentin, C. Di, Pacchioni, G., Onishi, H. & Kudo, A. Cr/Sb co-doped TiO2 from first principles calculations. *Chem. Phys. Lett.* **469,** 166–171 (2009).

110. Luo, H. *et al.* Photocatalytic Activity Enhancing for Titanium Dioxide by Co-doping with Bromine and Chlorine. *Chem. Mater.* **16,** 846–849 (2004).

111. Xiang, Q., Yu, J. & Jaroniec, M. Nitrogen and sulfur co-doped TiO $_2$ nanosheets with exposed {001} facets: synthesis, characterization and visible-light photocatalytic activity. *Phys. Chem. Chem. Phys.* **13,** 4853–4861 (2011).

112. Cong, Y., Tian, B. & Zhang, J. Improving the thermal stability and photocatalytic activity of nanosized titanium dioxide via La3+ and N co-doping. *Appl. Catal. B Environ.* **101,** 376–381 (2011).

113. Ye Cong, †, Jinlong Zhang, *,†, Feng Chen, †, Masakazu Anpo, ‡ and & He§, D.

Preparation, Photocatalytic Activity, and Mechanism of Nano-TiO2 Co-Doped with Nitrogen and Iron (III). (2007). doi:10.1021/JP0727493

114. Low, W. & Boonamnuayvitaya, V. Enhancing the photocatalytic activity of TiO2 co-doping of graphene–Fe3+ ions for formaldehyde removal. *J. Environ. Manage.* **127,** 142–149 (2013).

115. Yu, T. *et al.* Characterization, activity and kinetics of a visible light driven photocatalyst: Cerium and nitrogen co-doped TiO2 nanoparticles. *Chem. Eng. J.* **157,** 86–92 (2010).

116. Dai, K., Peng, T., Ke, D. & Wei, B. Photocatalytic hydrogen generation using a nanocomposite of multi-walled carbon nanotubes and TiO2 nanoparticles under visible light irradiation. *Nanotechnology* **20,** (2009).

117. Yao, Y., Li, G., Ciston, S., Lueptow, R. M. & Gray, K. a. Photoreactive TiO 2 /Carbon Nanotube Composites: Synthesis and Reactivity. *Environ. Sci. Technol.* **42,** 4952–4957 (2008).

118. Perera, S. D. *et al.* Hydrothermal Synthesis of Graphene-TiO $_2$ Nanotube Composites with Enhanced Photocatalytic Activity. *ACS Catal.* **2,** 949–956 (2012).

119. Huang, Z. *et al.* Effect of contact interface between TiO2 and g-C3N4 on the photoreactivity of g-C3N4/TiO2 photocatalyst: (0 0 1) vs (1 0 1) facets of TiO2. *Appl. Catal. B Environ.* **164,** 420–427 (2015).

120. Majek, M., Filace, F. & Wangelin, A. J. Von. On the mechanism of photocatalytic reactions with eosin Y. 981–989 (2014). doi:10.3762/bjoc.10.97

121. Wang, L., Zhao, H., Chen, Y., Sun, R. & Han, B. Efficient photocatalytic hydrogen production from water over Pt – Eosin Y catalyst : A systemic study of reaction parameters. *Opt. Commun.* **370,** 122–126 (2016).

122. Li, Q. *et al.* High-Efficient Photocatalytic Hydrogen Evolution on Eosin Y-

Sensitized Ti−MCM41 Zeolite under Visible-Light Irradiation. *J. Phys. Chem. C* **111,** 8237–8241 (2007).

123. Le, T. *et al.* Water splitting on Rhodamine-B dye sensitized Co-doped TiO2 catalyst under visible light. *Elsevier*

124. Jin, Z. *et al.* 5.1% Apparent quantum efficiency for stable hydrogen generation over eosin-sensitized CuO/TiO2 photocatalyst under visible light irradiation. *Elsevier*

125. Yin, M., Li, Z., Kou, J., technology, Z. Z.-E. science & & 2009, undefined. Mechanism Investigation of Visible Light-Induced Degradation in a Heterogeneous TiO2/Eosin Y/Rhodamine B System. *ACS Publ.*

126. Ehret, A., Stuhl, L. & Spitler, M. . Variation of carboxylate-functionalized cyanine dyes to produce efficient spectral sensitization of nanocrystalline solar cells. *Electrochim. Acta* **45,** 4553–4557 (2000).

127. Miyamoto, N., Kuroda, K. & Ogawa, M. Visible Light Induced Electron Transfer and Long-Lived Charge Separated State in Cyanine Dye/Layered Titanate Intercalation Compounds. *J. Phys. Chem. B* **108,** 4268–4274 (2004).

128. Gassim, F. A.-Z. G., Alkhateeb, A. N. & Hussein, F. H. Photocatalytic oxidation of benzyl alcohol using pure and sensitized anatase. *Desalination* **209,** 342–349 (2007).

129. Pei, D. & Luan, J. Development of visible light-responsive sensitized photocatalysts. *Int. J. Photoenergy* **2012,** (2012).

130. Tatsumi, K., Ichikawa, H. & Wada, S. Flavin-sensitized photooxidation of substituted phenols in natural water. *J. Contam. Hydrol.* **9,** 207–219 (1992).

131. Guo, M. *et al.* Photoelectrochemical studies of nanocrystalline TiO2 co-sensitized by novel cyanine dyes. *Sol. Energy Mater. Sol. Cells* **88,** 23–35 (2005).

132. Zong, R. & Thummel, R. P. A New Family of Ru Complexes for Water Oxidation. doi:10.1021/ja054791m

133. Teplý, F. Photoredox catalysis by [Ru(bpy)3]2+ to trigger transformations of organic molecules. Organic synthesis using visible-light photocatalysis and its 20th century roots. *Collect. Czechoslov. Chem. Commun.* **76,** 859–917 (2011).

134. Hong, D., Yamada, Y., Nagatomi, T., Takai, Y. & Fukuzumi, S. Catalysis of Nickel Ferrite for Photocatalytic Water Oxidation Using [Ru(bpy) $_3$] $^{2+}$ and S $_2$ O $_8$ $^{2-}$. *J. Am. Chem. Soc.* **134,** 19572–19575 (2012).

135. Khairutdinov, R., Chemistry, N. S.-T. J. of P. & 1999, undefined. Photoluminescence and transient spectroscopy of free base porphyrin aggregates. *ACS Publ.*

136. Rosenthal, J., Luckett, T., … J. H.-J. of the & 2006, undefined. Photocatalytic Oxidation of Hydrocarbons by a Bis-iron(III)-μ-oxo Pacman Porphyrin Using O2 and Visible Light. *ACS Publ.*

137. Wang, Z., Li, Z., … C. M.-J. of the A. & 2007, undefined. Self-assembly and self-metallization of porphyrin nanosheets. *ACS Publ.*

138. Fateeva, A. *et al.* A Water-Stable Porphyrin-Based Metal-Organic Framework Active for Visible-Light Photocatalysis. *Angew. Chemie* **124,** 7558–7562 (2012).

139. Pelaez, M. *et al.* A review on the visible light active titanium dioxide photocatalysts for environmental applications. *Appl. Catal. B Environ.* **125,** 331–349 (2012).

140. Gupta, S. M. & Tripathi, M. A review of TiO2 nanoparticles. *Chinese Sci. Bull.* **56,** 1639–1657 (2011).

141. Etacheri, V., Di Valentin, C., Schneider, J., Bahnemann, D. & Pillai, S. C. Visible-light activation of TiO2photocatalysts: Advances in theory and experiments. *J. Photochem. Photobiol. C Photochem. Rev.* **25,** 1–29 (2015).

142. Youngblood, W. J., Lee, S. A., Maeda, K. & Mallouk, T. E. Visible Light Water Splitting Using Dye- Sensitized Oxide Semiconductors. *Acc. Chem. Res.* **42,** 1966–1973 (2009).

143. Serpone, N., Chemistry, D. L.-… of P. & 1995, undefined. Size effects on the photophysical properties of colloidal anatase TiO2 particles: size quantization versus direct transitions in this indirect semiconductor? *ACS Publ.*

144. Wenderich, K. & Mul, G. Methods, Mechanism, and Applications of Photodeposition in Photocatalysis: A Review. *Chem. Rev.* **116,** 14587–14619 (2016).

145. Clark, W., Catalysis, A. V.-J. of & 1965, undefined. An infrared study of the photocatalytic reaction between titanium dioxide and silver nitrate. *Elsevier*

146. Kanda, S., Akita, T., Fujishima, M., interface, H. T.-J. of colloid and & 2011, undefined. Facile synthesis and catalytic activity of MoS2/TiO2 by a photodeposition-based technique and its oxidized derivative MoO3/TiO2 with a unique. *Elsevier*

147. Fujii, M., Nagasuna, K., … M. F.-T. J. of & 2009, undefined. Photodeposition of CdS Quantum Dots on TiO2: Preparation, Characterization, and Reaction Mechanism. *ACS Publ.*

148. Forouzan, F., Richards, T. C. & Bard, A. J. Photoinduced Reaction at TiO_2 Particles. Photodeposition from Ni^{II} Solutions with Oxalate. *J. Phys. Chem.* **100,** 18123–18127 (1996).

149. Chan, S., Langmuir, M. B.- & 2005, undefined. Preparation of Highly Uniform Ag/TiO2 and Au/TiO2 Supported Nanoparticle Catalysts by Photodeposition. *ACS Publ.*

150. Sliem, M. *et al.* Interfacial Cu/ZnO contact by selective photodeposition of copper onto the surface of small ZnO nanoparticles in non-aqueous colloidal solution. *pubs.rsc.org*

151. Behnajady, M., Modirshahla, N., … M. S.-… S. and H. & 2009, undefined. Enhancement photocatalytic activity of ZnO nanoparticles by silver doping with optimization of photodeposition method parameters. *Taylor Fr.*

152. Liu, Y., Wei, S. & Gao, W. Ag/ZnO heterostructures and their photocatalytic activity under visible light: Effect of reducing medium. *J. Hazard. Mater.* **287,** 59–68 (2015).

153. Widiyandari, H., Purwanto, A., Balgis, R., … T. O.-C. E. & 2012, undefined. CuO/WO3 and Pt/WO3 nanocatalysts for efficient pollutant degradation using visible light irradiation. *Elsevier*

154. Karácsonyi, É. *et al.* The photocatalytic activity of TiO2/WO3/noble metal (Au or Pt) nanoarchitectures obtained by selective photodeposition. *Elsevier*

155. Li, Y., Wang, H. & Peng, S. Tunable Photodeposition of MoS $_2$ onto a Composite of Reduced Graphene Oxide and CdS for Synergic Photocatalytic Hydrogen Generation. *J. Phys. Chem. C* **118,** 19842–19848 (2014).

156. Dukovic, G., Merkle, M., … J. N.-A. & 2008, undefined. Photodeposition of Pt on colloidal CdS and CdSe/CdS semiconductor nanostructures. *Wiley Online Libr.*

157. Ishii, T., Kato, H., A, A. K.-J. of P. and P. & 2004, undefined. H2 evolution from an aqueous methanol solution on SrTiO3 photocatalysts codoped with chromium and tantalum ions under visible light irradiation. *Elsevier*

158. Miyauchi, M., Takashio, M., Langmuir, H. T.- & 2004, undefined. Photocatalytic Activity of SrTiO3 Codoped with Nitrogen and Lanthanum under Visible Light Illumination. *ACS Publ.*

159. Ohsawa, T., Nakajima, K., science, Y. M.-A. surface & 2006, undefined. Combinatorial discovery of anomalous substrate effect on the photochemical properties of transition metal-doped epitaxial SrTiO3 heterostructures. *Elsevier*

160. Yoshida, M., Yomogida, T., Mineo, T., … K. N.-C. & 2013, undefined. In situ

observation of carrier transfer in the Mn-oxide/Nb: SrTiO3 photoelectrode by X-ray absorption spectroscopy. *pubs.rsc.org*

161. Behnajady, M., Modirshahla, N., … M. S.-G. N. & 2008, undefined. Enhancement of photocatalytic activity of TiO2 nanoparticles by silver doping: photodeposition versus liquid impregnation methods. *journal.gnest.org*

162. Byrappa, K. *et al.* Impregnation of ZnO onto activated carbon under hydrothermal conditions and its photocatalytic properties. *J. Mater. Sci.* **41,** 1355–1362 (2006).

163. Zhang, W., Zou, L., General, L. W.-A. C. A. & 2009, undefined. Photocatalytic TiO2/adsorbent nanocomposites prepared via wet chemical impregnation for wastewater treatment: A review. *Elsevier*

164. Li, X. *et al.* Photocatalytic degradation of gaseous toluene over Ag-doping TiO2 nanotube powder prepared by anodization coupled with impregnation method. *Elsevier*

165. Nasution, H., Purnama, E., … S. K.-C. & 2005, undefined. Photocatalytic reduction of CO2 on copper-doped Titania catalysts prepared by improved-impregnation method. *Elsevier*

166. Miller, J. T., Schreier, M., Kropf, A. J. & Regalbuto, J. R. A fundamental study of platinum tetraammine impregnation of silica: 2. The effect of method of preparation, loading, and calcination temperature on (reduced) particle size. *J. Catal.* **225,** 203–212 (2004).

167. Kohtani, S., Hiro, J., Yamamoto, N., … A. K.-C. & 2005, undefined. Adsorptive and photocatalytic properties of Ag-loaded BiVO4 on the degradation of 4-n-alkylphenols under visible light irradiation. *Elsevier*

168. Wang, Z., Hou, J., Jiao, S., Huang, K. & Zhu, H. In situ chemical reduction of the Ta3N5 quantum dots coupled TaON hollow spheres heterojunction photocatalyst for water oxidation. *J. Mater. Chem.* **22,** 21972 (2012).

169. Zhu, H. & Sadoway, D. R. Synthesis of nanoscale particles of Ta and Nb3Al by homogeneous reduction in liquid ammonia. *J. Mater. Res.* **16,** 2544–2549 (2001).

170. Wang, Y. *et al.* Fabrication of nanostructured CuO films by electrodeposition and their photocatalytic properties. *Elsevier*

171. Zhang, S. *et al.* Electrodeposition preparation of Ag loaded N-doped TiO2 nanotube arrays with enhanced visible light photocatalytic performance. *Elsevier*

172. Wang, J. *et al.* Cu2O/TiO2 heterostructure nanotube arrays prepared by an electrodeposition method exhibiting enhanced photocatalytic activity for CO2 reduction to methanol. *Elsevier*

173. Wei, S., Chen, Y., Ma, Y., Chemical, Z. S.-J. of M. C. A. & 2010, undefined. Fabrication of CuO/ZnO composite films with cathodic co-electrodeposition and their photocatalytic performance. *Elsevier*

174. Kleiman-Shwarsctein, A., … Y. H.-T. J. of & 2008, undefined. Electrodeposition of α-Fe2O3 Doped with Mo or Cr as Photoanodes for Photocatalytic Water Splitting. *ACS Publ.*

175. Kang, J. G. & Sohn, Y. Interfacial nature of Ag nanoparticles supported on TiO 2 photocatalysts. *J. Mater. Sci.* **47,** 824–832 (2012).

176. Lu, J., Elam, J. W. & Stair, P. C. Atomic layer deposition - Sequential self-limiting surface reactions for advanced catalyst ‘bottom-up’ synthesis. *Surf. Sci. Rep.* **71,** 410–472 (2016).

177. Zhou, Y., King, D. M., Liang, X., Li, J. & Weimer, A. W. Optimal preparation of Pt/TiO2 photocatalysts using atomic layer deposition. *Appl. Catal. B Environ.* **101,** 54–60 (2010).

178. Liang, Y., Wang, C., Kei, C., … Y. H.-T. J. of & 2011, undefined. Photocatalysis of Ag-Loaded TiO2 Nanotube Arrays Formed by Atomic Layer Deposition. *ACS Publ.*

179. Gould, T. D. *et al.* Synthesis of supported Ni catalysts by atomic layer deposition. *J. Catal.* **303,** 9–15 (2013).

180. Kayaci, F., Ozgit-Akgun, C., … I. D.-A. applied materials & 2012, undefined. Polymer–inorganic core–shell nanofibers by electrospinning and atomic layer deposition: flexible Nylon–ZnO core–shell nanofiber mats and their photocatalytic. *ACS Publ.*

181. Liu, C., Wang, C.-C., Kei, C.-C., Hsueh, Y.-C. & Perng, T.-P. Atomic Layer Deposition of Platinum Nanoparticles on Carbon Nanotubes for Application in Proton-Exchange Membrane Fuel Cells. *Small* **5,** 1535–1538 (2009).

Chapter 3

3 Hydrogen Generation from Eosin Y-sensitized Pt/ZnO under Solar Light Irradiation

3.1 Introduction

The upcoming depletion of fossil fuel and the increasing frequency of disasters caused by global warming and climate change make finding a new, clean and renewable energy essential for human society.[1,2] Hydrogen, is a promising future energy carrier for it is clean, efficient and abundant on Earth (in combination form).[3] The current most extensively used technique for hydrogen production is steam reforming of methane.[4] Although compared to other existing techniques, such as partial oxidation and autothermal reforming, steam reforming has advantages of low reacting temperature and best H_2/CO ratio for hydrogen production, it has the highest air emission which is harmful to the environment.[5,6]

Hydrogen is vastly distributed and abundant element on Earth but it always in combination with other elements. Water occupies for more than seventy percent of the Earth area composed of hydrogen and oxygen element. Therefore, if hydrogen could be separated from water with efficiency that high enough for commercial use, the energy crisis of our era could be greatly relieved.

In 1972, TiO_2 was first studied as photocatalyst to produce hydrogen by A. Fujishima and K. Honda.[7] The band gap of TiO_2 is 3.2 eV which is too large for it to be activated under visible light irradiation and can only be triggered under wavelength shorter than 387 nm (UV light section).[8,9] However, visible light accounts for 46% of the solar energy while ultra-violet (UV) only accounts for 4% of the solar energy.[10] Therein, massive waste of solar energy can be caused for the reasons above. Since then, photocatalytic activity of numerous materials for hydrogen generation have been tested, such as Fe_2O_3-based photocatalyst[11], WO_3-based photocatalyst[12], and C_3N_4-based photocatalyst[13], but few materials have the capacity to split water under visible light irradiation with high efficiency.

Water splitting is a difficult process because it is an uphill reaction, as shown in eq. (3.1).

$$H_2O \rightarrow H_2 + \frac{1}{2}O_2 \qquad \Delta G = +237.2\ \mathrm{KJ/mol} \tag{3.1}$$

The successful initiation of water splitting reaction requires the band gap of photocatalysts to be larger than 1.23eV[14]. The wavelength of visible light is longer than 415 nm, so the band gap of photocatalyst should be narrower than 3.0 eV.[15] . The relation between wavelength and band gap was shown in eq. (3.2). In the ideal situation, the position of conduction band of semiconductor need to be higher than the reduction potential of hydrogen evolution reaction (HER) that reduce H^+ to H_2 molecules while the position of valence band of semiconductor should be lower than the oxidation potential of oxygen evolution reaction (OER) that oxidize H_2O to O_2.[16–19] The strict requirements for band gap and band positions of photocatalysts have greatly hindered their application.

$$\text{Band gap (eV)} = 1240/\lambda\ \text{(nm)} \tag{3.2}$$

According to literature, recombination of e^-/h^+ can happen in microseconds to miliseconds[20]. Fast recombination of electrons and holes inside the bulk of catalyst is also one of the main factors that limit the efficiency of photocatalyst.

Dyes can act as photosensitizers which could absorb visible slight so that photocatalysts with inappropriate band gap or band position could be reactive under solar light irradiation. Therefore, light energy utilization can be greatly enlarged. Organic dyes, such as erythrosin B,[21,22] eosin Y[23–25] and cyanines,[9,26,27] have been proved to be efficient in improving sunlight harvesting, low toxicity and prominent photo-physical properties. Besides, dye molecules can transit to excited states fast to produce excited electrons followed by fast injection to the conduction band of semiconductors which happen in femtoseconds. Therefore, effectively separate excited electrons can be achieved for the fast electron injection and relatively slow recombination (backward) reaction. Sacrificial reagent TEOA was applied in the system to prolong the lifetime of the dye molecules. Many investigations have been invested on sacrificial donors, and triethanolamine (TEOA),[28,29] ethanol[30] and methanol[31–33] are extensively used as sacrificial reagents in this field.[34]

Cocatalyst is an important method of band gap engineering, for the contact between the metal and the semiconductor creates an electric field that separates excited electrons and holes more easily [35]. Platinum, which was commonly used as cocatalyst, can dramatically increase photocatalytic activity of semiconductors because it can provide reductive sites for hydrogen generation reaction to occur as well as attract electrons to migrate to Pt sites with its low fermi energy level to effectively enhance e^-/h^+ separation.

In this study, ZnO was chosen as host catalyst for it has higher carrier mobility compared with TiO_2. We aim to investigate the activity of Eosin Y-sensitized Pt/ZnO under both visible light (λ>415 nm) and solar light irradiation in different conditions. Platinum was loaded onto zinc oxide via photodeposition method. (i) PH value, (ii) platinum loading content, (iii) Eosin Y concentration, (iv) TEOA concentration, (v) solar light and visible light density, (vi) photocatalyst loading are the six factors that were investigated on their effect to hydrogen production. Possible mechanism was discussed in this paper. This study could shed some light on optimization of photocatalyst study and realization of large-scale fuel production.

3.2 Experimental Section

3.2.1 Chemicals

Zinc Oxide (99.7+% pure) was purchased from Inframat Advanced Materials and was used as photocatalyst. Eosin Y dye (99.0% pure) was purchased from Sigma–Aldrich Canada Ltd and was used as the photosensitizer. Triethanolamine (98.0% pure), procured from Sigma–Aldrich Canada Ltd was used as sacrificial electron donor. Hydrogen hexachloroplatinate (IV) solution (8 wt%, Sigma–Aldrich Canada Ltd) was used as precursor in the process of photo-deposition to load platinum onto zinc oxide. All chemicals were of analytical grade and were used without any further treatment.

3.2.2 Preparation of Pt/ZnO

Platinum loaded zinc oxide was prepared by photo-deposition method.[36] Typically, zinc oxide powder was added into the solution of ethanol and water with the volume ratio of 10: 90, where ethanol acted as electron donor to assist the photo-reduction of

hexachloroplatinate (IV) to Pt. Hexachloroplatinate (IV) solution (8 wt%) was then added to the suspension with the amount calculated by nominal loading. The suspension was kept under the irradiation of solar light in power of 100 mW cm^{-2} (1 sun) for 3h with consistent stirring. After filtering and washing, particles were collected and dried at 150°C in the oven for 150 min and then milled in a mortar to obtain the final model photocatalyst, Pt/ZnO with different nominal platinum loadings (0.25w%-1.5w%). As photo-deposition went on, the color of photocatalyst gradually changed from white to grey because of the loading of platinum.

3.2.3 Photocatalytic characterization

XRD was used to characterize and analyze the phase composition and the degree of crystallinity of Pt/ZnO. Rigaku−MiniFlex II powder diffractometer at 40 kV and 40 mA with Cu Kα irradiation was used to collect data. The spectra was recorded in scanning speed of 2.00°/min and step width of 0.020° over the 2θ range of 20 to 80° (where λ for Kα= 1.54059Å, θ= Bragg angle). Diffuse reflectance spectra (DRS) was conducted by UV-3600 SHIMADZU equipped with a Praying Mantis to analyses the ability of photocatalyst to absorb light with various wavelength. Scanning electron microscope (SEM) with energy dispersive X-ray (EDX) analysis was performed to study the morphology of photocatalyst as well as to identify the elements contained in the photocatalyst. Brunauer−Emmett−Teller (BET) specific surface area of Pt/ZnO was measured by Micromeritics ASAP 2010 instrument via N_2 adsorption method.

3.2.4 Photocatalytic experiment

A gas-tight Pyrex glass (530 mL) batch reactor was used for photocatalysis experiments. The reactor was 55 mm in diameter and 63 mm in height. It has a transparent flat window at the top to allow solar light to illuminate the reactant mixture. A solar simulator (model SS1KW, Sciencetech) equipped with a 1000 W Xe arc lamp, was used as the light source. It contains a 420 nm cut-off filter (Omega optical, USA), to remove UV light from the entire solar spectrum, and a 1.5G AM filter. The maximum power of simulated solar light that can be reached is 100 mW cm^{-2} which resembles 1 sun light intensity at sea level.

100 mg of prepared Pt/ZnO photocatalyst was suspended in 100 mL solution of TEOA and Eosin Y (1:10 volume%). Here TEOA acts as the sacrificial agent and EosinY as the photosensitizer. The pH is then adjusted using 1:1 HCl and 1:1 NaOH (volume ratio) and sonicated for 10 min in an ultrasonic bath. Ultra-pure nitrogen was purged into the system for 40 min to get rid of any air inside the reactor and suspension. The reactor was put at the center of irradiation area of the light with consistent vigorous stirring. To ensure the gas tightness of the system, a silicone rubber septum was used to seal the reactor while allowed sampling to be done by microsyringe (1 mL) every 30 min. The sample was then injected into the sample port of GC (Shimazu 2014, HeyeSep D packed column: 10 m length, 2 mm ID, 2mm film thickness and thermal conductivity detector(TCD)) to be analyzed and N_2 was used as carrier gas.[37]

3.3 Results and discussion

3.3.1 Characterization of Pt/ZnO

The XRD pattern shown in Fig. 3.2 and Fig 3.3 were used to demonstrate difference between the crystallinity and phase before and after and loading of platinum. The peaks

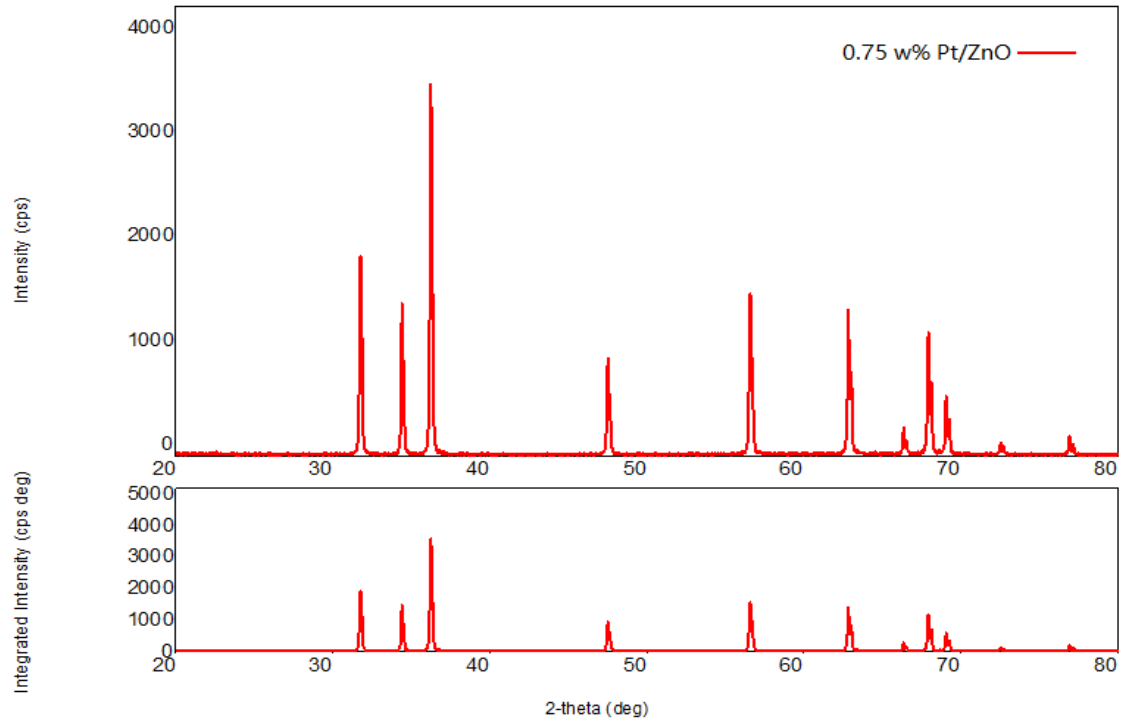

Figure 3. 1 XRD of 0.75 w% Pt/ZnO

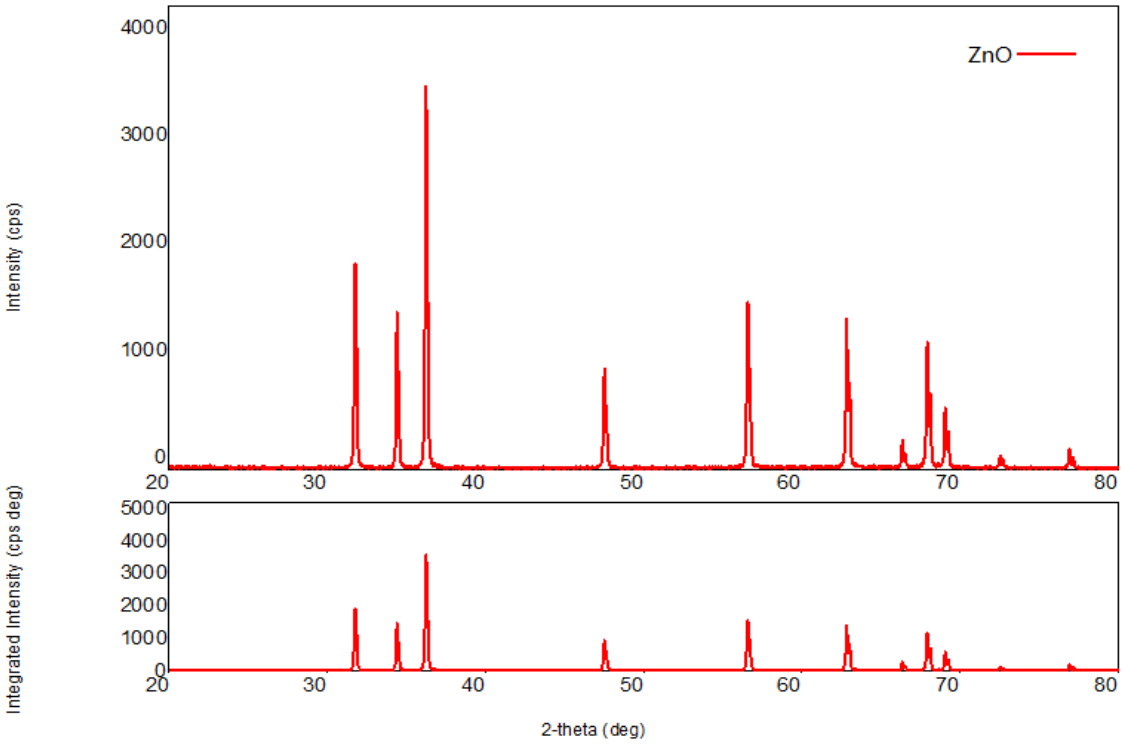

Figure 3. 2 XRD of pure ZnO

at 2θ= 31.680, 34.340, 36.180, 47.480, 56.540, 62.780° are observed and the calculated d-value agree with standard data of zinc acetate (JCPDS, 36-1451) which revealed the high crystallinity of the sample. The comparison between ZnO and Pt/ZnO showed almost no obvious difference which means that the loading of platinum didn't significantly alter the crystallinity and phase of the photocatalyst.

The DRS spectra shown in fig. aims to investigate the absorption wavelength and band gap of the Pt/ZnO and pure ZnO. From the Fig. 3.4, it can be said, that the maximum wavelength of light needed for ZnO to excite is around 376 nm which is consistent with the calculated result of wavelength from eq. (3), as the band gap of ZnO being 3.3 eV. After loading platinum, the band gap of photocatalyst didn't change much. However, it could still be observed that a small red shift has occurred due to platinum loading.

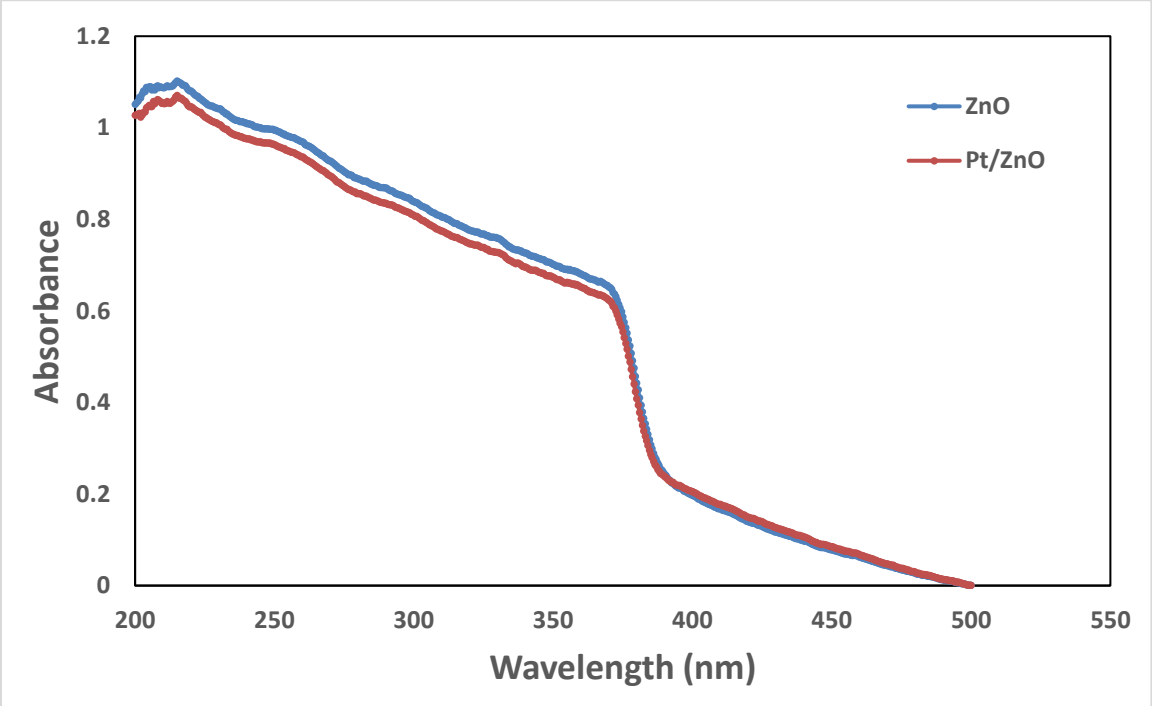

Figure 3. 3 DRS of 0.75 w% Pt/ZnO and ZnO

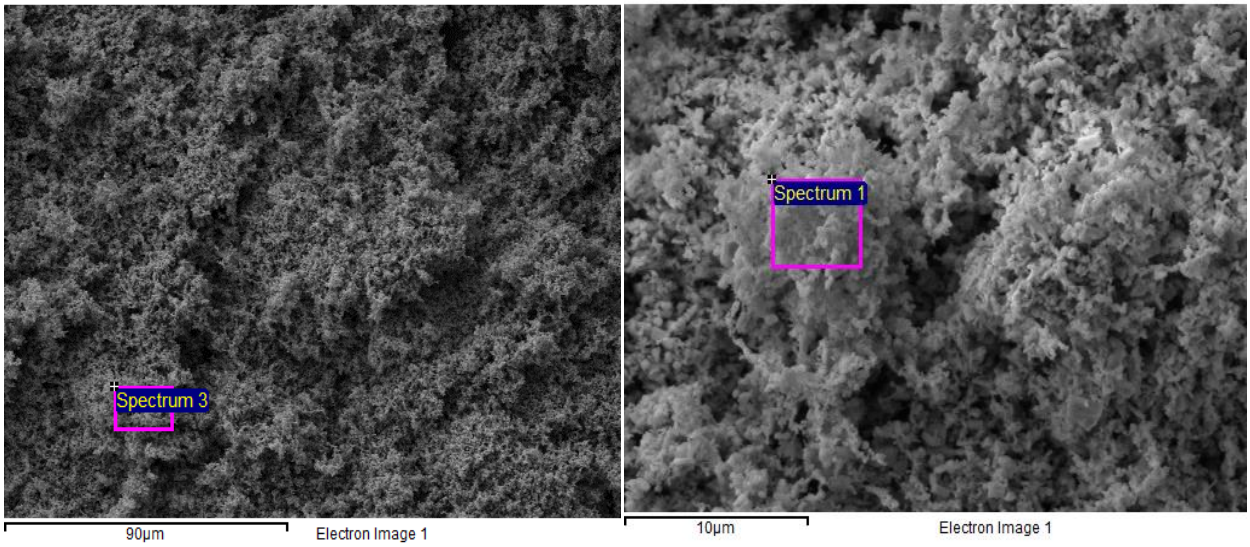

Figure 3. 4 SEM of 0.75 w% Pt/ZnO

The morphology of the photocatalysts were analyzed by SEM followed by EDX to determine the weight percentages of elemental composition. The SEM results are shown in fig. 3.5. From SEM analysis, the difference between the morphology of ZnO and Pt/ZnO seems not significant. In both cases, particles are uniformly distributed, and no agglomerates could be observed by SEM. No obvious morphology changes were observed. However, it has been reported before that the increased loading of platinum will increase the appearance of regular microspheres.[38] The EDX analysis confirmed the presence of Pt in the prepared photocatalyst as shown in Fig. 3.6. As expected, it contains large amount of Zn and O, along with a small amount of Pt and carbon.

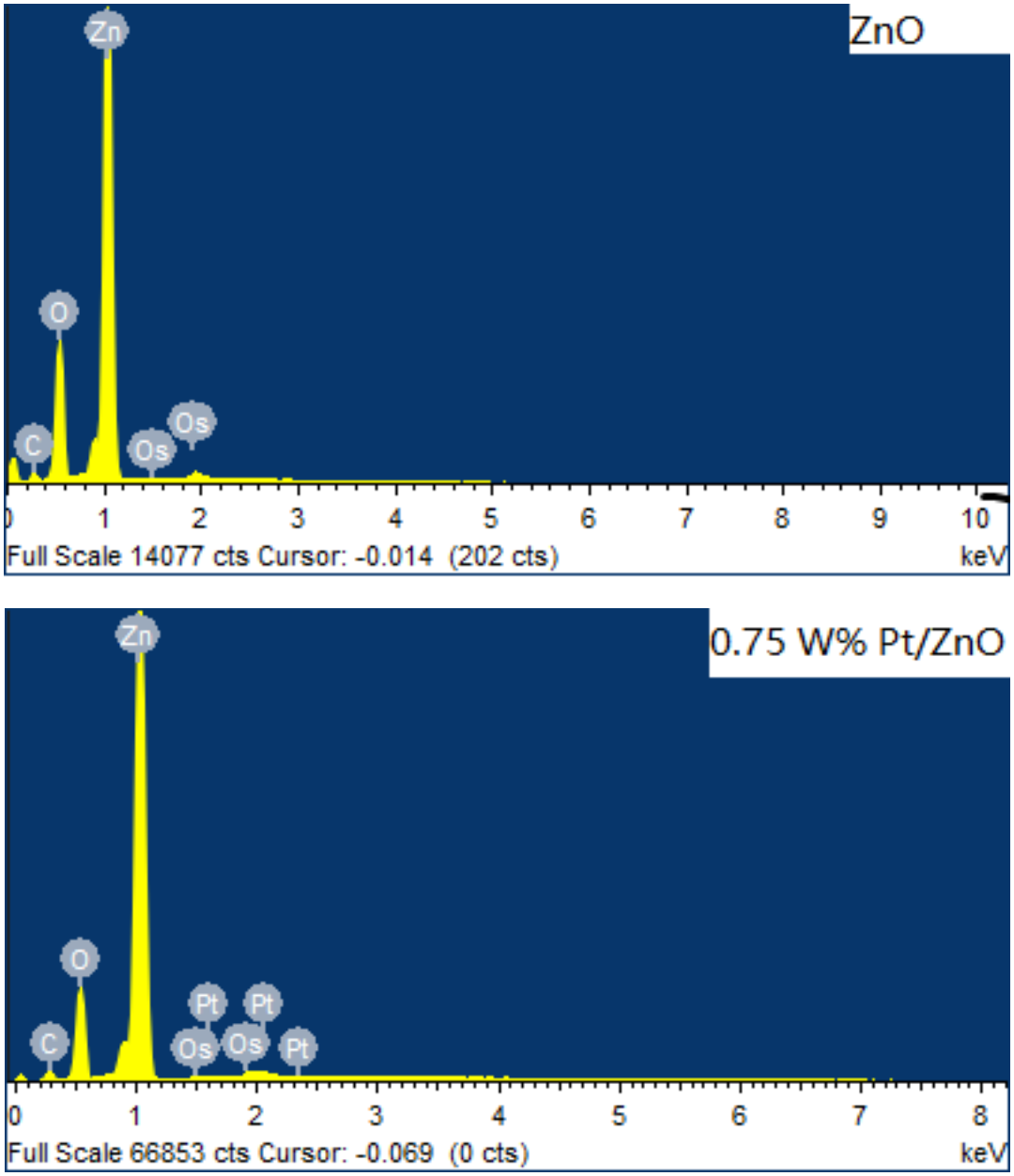

Figure 3. 5 EDX of ZnO and 0.75 w% Pt/ZnO

BET specific surface area were measured before and after Pt loading which were 2.9895 m^2/g and 3.8681 m^2/g. The result shows that the loading of Pt didn't significantly enlarge the specific surface area.

3.3.2 Possible mechanism of hydrogen generation from Pt/ZnO

Considering the band gap of ZnO to be 3.3 eV, the maximum wavelength of light to activate ZnO is calculated to be 376 nm. The band gap of the photocatalyst shows no significant change after loading of platinum on ZnO. Therefore, visible light cannot activate Pt/ZnO in absence of EY. EY can absorb long wavelength light and inject electrons into photocatalyst. Firstly, dye molecules transit to excited states by absorbing photons from light illumination as shown in eq. (5).[39] During this step, electrons transit from the highest occupied molecular orbital (HOMO) to the lowest occupied molecular orbital (LUMO) of the dye molecules that absorbed onto the surface of semiconductors. Dye molecules in excites states can generate excited electrons as shown in eq. (6).[39] The excited electrons can then migrate to the conduction band of host photocatalysts to participate HER. In our case, the fermi energy level of Pt as co-catalyst is relatively low so the excited electrons will transfer to the Pt sites of photocatalyst instead as shown in eq. (7-9).

$$\mathrm{Dye} \xrightarrow{h\nu} \mathrm{Dye}^{*} \tag{5}$$

$$\mathrm{Dye}^{*} \rightarrow \mathrm{Dye}^{+} + \mathrm{e}^{-} \tag{6}$$

Moreover, electron-hole recombination happens in nanoseconds to microseconds while electron injection from dye molecules to photocatalysts happens in femtoseconds.[40] The fast injection rate can hinder the electron-hole recombination which further improve the excited electrons and holes separation and promote HER.[41]

Considering EY can be activated by light with maximum wavelength of 535nm,[42] the scheme of mechanism can be divided into two section, which is λ<535 nm (in visible light section, eq. (7-10)) and λ<376 nm (in UV light section, eq. (11-16)).[25]

$$\mathrm{ZnO} - (\mathrm{EY})_s \xrightarrow{h\nu(\lambda<535\ nm)} \mathrm{ZnO} - (\mathrm{EY}^{*})_s \tag{7}$$

$$\mathrm{ZnO} - (\mathrm{EY}^{*})_s \xrightarrow{h\nu} \mathrm{ZnO} - (\mathrm{EY}^{+} + \mathrm{e}^{-})_s \tag{8}$$

$$\mathrm{ZnO} - (\mathrm{EY}^{+} + \mathrm{e}^{-})_s + \mathrm{Pt} \rightarrow \mathrm{ZnO} - (\mathrm{EY}^{+})_s + \mathrm{Pt}(\mathrm{e}^{-}) \tag{9}$$

$$Pt(e^-) + H_2O \rightarrow Pt + \frac{1}{2}H_2 + HO^- \quad (10)$$

$$ZnO - (EY)_s \xrightarrow{hv(\lambda<376\ nm)} ZnO(h^+ + e^-) - (EY)_s \quad (11)$$

$$ZnO(h^+) + HO^- \rightarrow ZnO + HO^{\cdot} \quad (12)$$

$$ZnO(h^+) + H_2O \rightarrow ZnO + HO^{\cdot} + h^+ \quad (13)$$

$$ZnO - (EY^+ + e^-)_s + TEOA \rightarrow ZnO - (EY + e^-)_s + TEOA^+ \quad (14)$$

$$TEOA + HO^{\cdot} \rightarrow HCHO + NH_3 + H_2O \quad (15)$$

$$HCHO + HO^{\cdot} \rightarrow\rightarrow H_2 \quad (16)$$

3.3.3 Effect of platinum loadings on photocatalytic activity of ZnO

Several experiments are conducted to test the influence of platinum loading content on photocatalytic activity of ZnO. In comparison to the photocatalytic activities of Pt/ZnO, reference experiments were conducted using pure ZnO as photocatalysts in the same conditions under both solar and visible light irradiation (10 v% TEOA, pH =7, 100 mW/cm^2 light intensity, 50 mg EY). The result shows that ZnO without platinum loading was not reactive under solar and visible light irradiation. However, in the same experimental condition, Pt/ZnO was not only reactive under both solar and visible light irradiation but also have relatively high photocatalytic activity in both cases. Different loading content of Pt onto ZnO were studied here (0.25 wt%, 0.5 wt%, 0.75 wt%, 1.0 wt%, 1.25 wt% and 1.5 wt. The dependence of the amount of platinum loading to hydrogen generation rate was shown in Fig. 3.7.

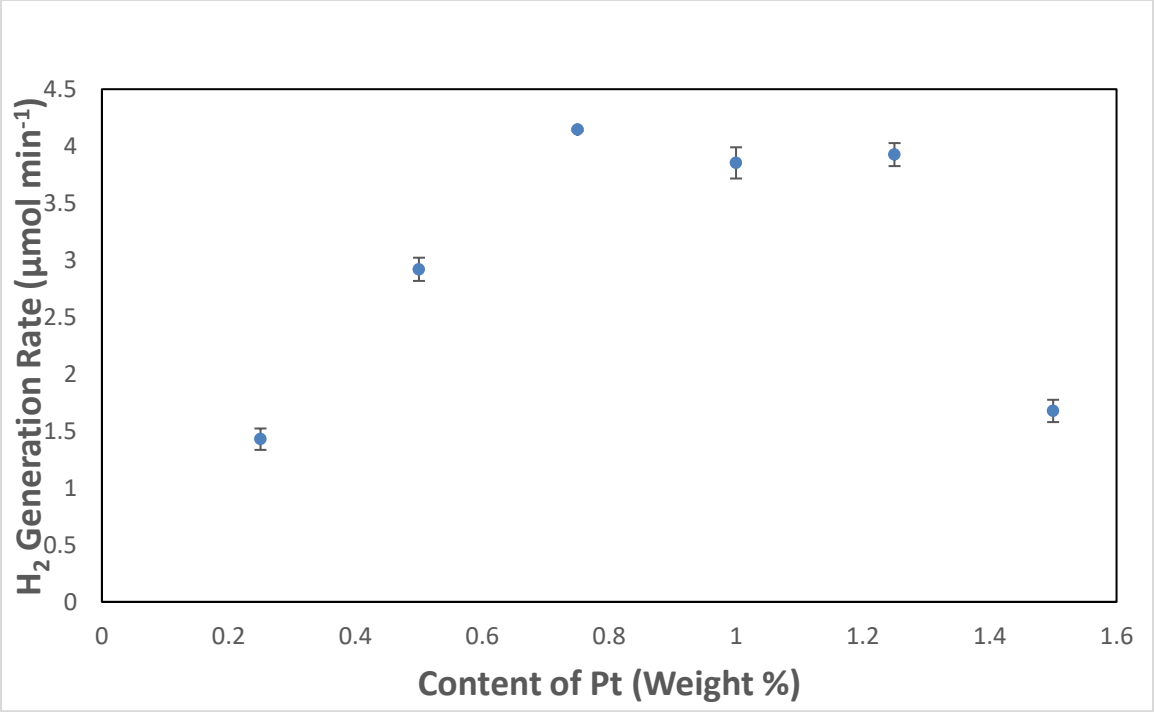

Figure 3. 6 Dependence of Pt loading to hydrogen generation rate

As mentioned before, the easy occurring of recombination reaction driven by the large negative value of Gibbs free energy in thermodynamic view is one of the main reasons of the low hydrogen production rate. In this case, the increase of hydrogen generation rate may be explained by hindering recombination of excited electrons and holes as well as larger specific surface area confirmed by BET test. Loading of platinum onto ZnO offers efficient reduction sites for HER because Fermi levels of platinum and the overpotential for HER on a Pt co-catalyst is favorably low. Low Fermi energy level can attract excited electrons to migrate to Pt sites which promotes excited electron-hole separation. Low overpotential for HER allows the HER to become thermodynamically favorable. Therefore, with the loading of Pt, electrons can be continuously pumped into reduction sites to promote the occurring of HER. The decrease in the hydrogen generation rate may be explained by ZnO crystallinity damaging and clusters forming on the surface of photocatalyst caused by excessive loading of platinum which promote the forming of charge recombination center and thereby speeding up the recombination rate.[43] Loss of light energy caused by increasing light scattering from platinum loading sites and

decreasing light absorbing area may also be a factor for decreasing hydrogen generation rate.[44]

3.3.4 Effect of solar and visible light intensity on hydrogen generation rate

The hydrogen generation rate largely depends on the absorbance of solar light. Therefore, theoretically, the increased solar light intensity will result in increasing hydrogen generation rate which is consistent with the actual result we got, as shown in Fig. 3. Keeping concentration of TEOA and EY, pH value fixed (10 v% TEOA, pH=7, 1.0 g l^{-1} catalyst loading, 50 mg EY) and the system was under the irradiation with light intensity of 300 mW cm^{-2}, 500 mW cm^{-2}, 800 mW cm^{-2}, and 1000 mW cm^{-2}, and the hydrogen generation rate was calculated respectively. The result shows although hydrogen generation rate is higher under solar light irradiation in comparison to visible light irradiation, but the difference is not significantly large.

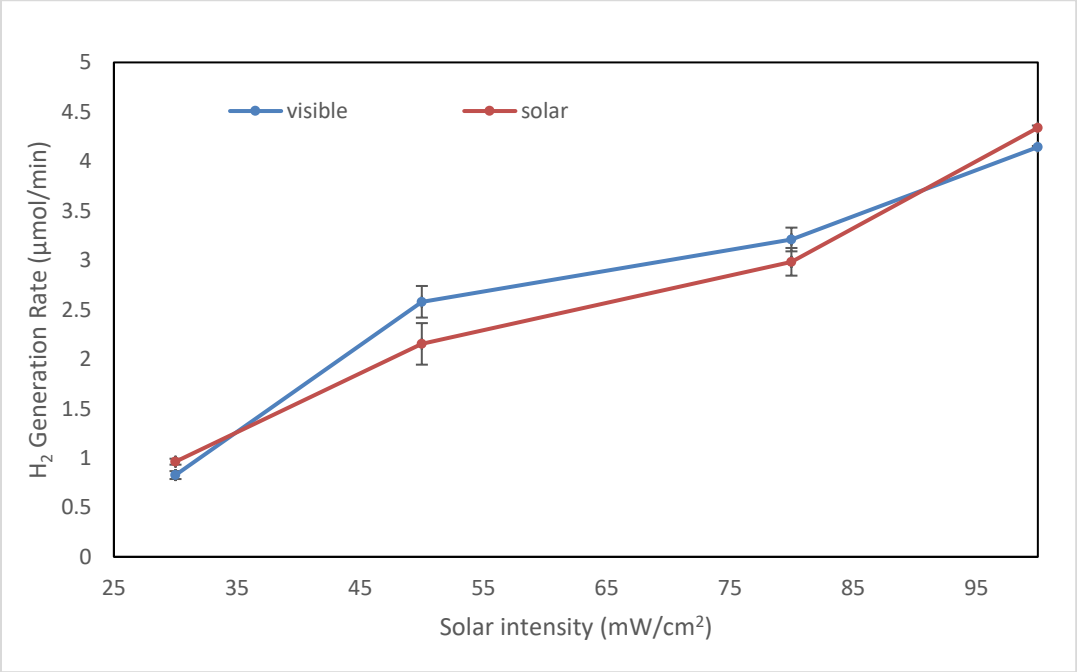

Figure 3. 7 Dependence of solar and visible light intensity to hydrogen generation

3.3.5 Effect of initial pH on photocatalytic activity of Pt/ZnO

Hydrogen generation rate increased sharply with the increase of pH value from 5 to 7, reaching maximum at pH =7 and started decreasing afterwards. The pH value can greatly affect the hydrogen generation rate since the formation of hydroxyl radicals and H^+ depends on the surface charge of semiconductor, which is ultimately governed by the pH of the mixture of reactants. To study the effect of initial pH, the concentration of EY and TEOA, catalyst loading and light intensity were all kept constant while only changing the pH value of the system (10 v% TEOA, 1.0 g l^{-1} catalyst loading, 100 mW/cm^2 light intensity, 50 mg EY).

The surface of ZnO can be positively or negatively charged in different values of pH. Based on the studies conducted before, the zero-point charge (zpc) for ZnO is at pH 9.0±0.3, which may be slightly altered by loading of platinum.[45–47] Therefore, the surface of ZnO is positively charged when pH is below 9.0 and negatively charged when pH is above 9.0.

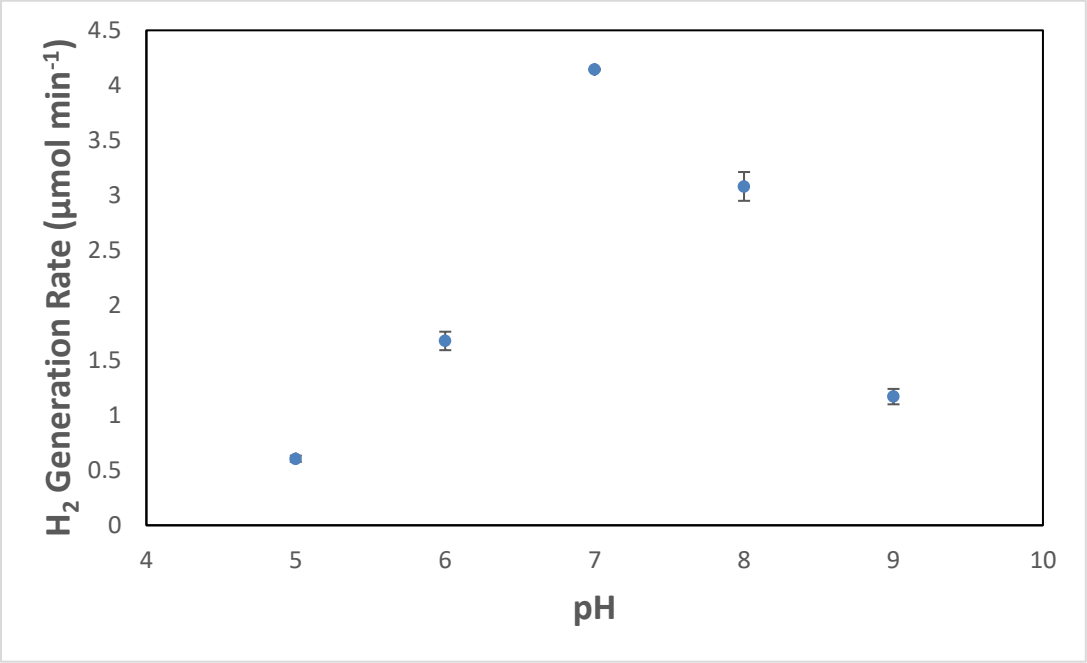

Figure 3. 8 Dependence of pH value to hydrogen generation rate

The results obtained here can be explained by the acid-base properties of ZnO surface and the role of TEOA in the process of photocatalytic reaction. Eosin Y is an acidic dye.[42,48] In acidic environment, Eosin Y exists as EY dianion, which means the electro-interaction between positively charged ZnO surface and EY anion is strong, resulting in the stronger absorbance of EY dyes to the surface of ZnO. However, TEOA will be protonated which would hinder its electron donating ability in low pH value.[49] Moreover, based on several studies, the possible mechanism of ZnO corrosion can be expressed by eq. (11-14).[50–52] Therefore, acid system condition could have negative effect on the stability of ZnO as photocatalyst.

$$O^{2-}_{surface} + h^{+} = O^{-}_{surface} \tag{11}$$

$$O^{-}_{surface} + 3O^{2-} + 3h^{+} = 2(O - O^{2-}) \tag{12}$$

$$O - O^{2-} + 2h^{+} = O_2 \tag{13}$$

$$2Zn^{2+} \rightarrow 2Zn^{2+}_{aq} \tag{14}$$

On the other hand, at basic pH, HER becomes thermodynamically unfavorable because the driving force of HER decreases. The electrostatic repulsion between negatively charged surface of ZnO and EY dianion hinders the injection of excited electrons from dyes to photocatalyst. Protons which play the essential role in the HER process will decrease as protonation of co-catalyst gets difficult in high pH value. Besides, strong basicity can have negative implication on the integrity of photocatalyst.[29]

3.3.6 Effect of initial TEOA concentration

TEOA was a type of commonly used hole scavenger for it has irreversible oxidation potentials around 0.7 V vs. SCE.,[29,22,53] making it thermodynamically favorable for hole consuming. The effect of initial TEOA concentration on hydrogen generation rate has been studied by varying the concentration of TEOA while keeping other parameters constant, under both visible light and solar light irradiation. The result is shown in Fig.3.11. The result shows that hydrogen generation rate increased with increasing TEOA

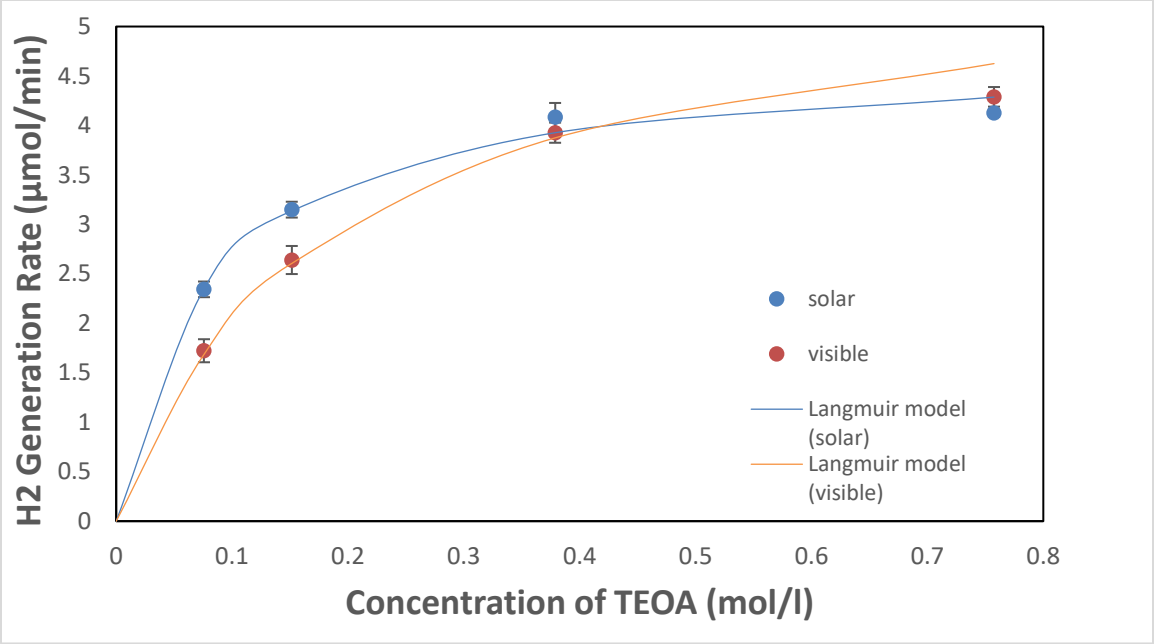

Figure 3. 9 Dependence of volume concentration of TEOA to hydrogen generation

concentration. The increase in rate was relatively large before TEOA concentration reached 5 v% (0.379 mol l^{-1}), after which hydrogen generation rate started to increase slowly in both cases. The difference of hydrogen generation rate under solar and visible light irradiation gets smaller with increment of TEOA concentration. TEOA plays an important role in photocatalytic activities of Pt/ZnO for two main reasons. On one hand, as mentioned before, it can react with excited holes to inhibit electron-hole recombination reaction which helps to promote HER. On the other hand, it can provide electrons to EY cation radicals to regenerate EY, improving the stability of the system.[54]

It has been reported that the most extensively used reaction kinetic model for photocatalytic reactions is Langmuir-Hinshelwood kinetic model as shown below.[55–57]

$$\mathrm{r} = -\frac{dC_{H_2}}{dt} = \frac{kKC}{1+KC} \tag{15}$$

From the results, the dependence of hydrogen generation rate and TEOA concentration is not linear and the increasing rate keeps decreasing along with the increasing of TEOA concentration, and Langmuir-Hinshelwood kinetic model can fit well with the above two

variables with K_{solar}= 13.080 M^{-1}, k_{solar}= 4.719 × 10^{-6} mol min^{-1} in solar light irradiation and $K_{visible}$= 5.491 M^{-1}, $k_{visible}$= 5.738 × 10^{-6} mol min^{-1} in visible light irradiation respectively as shown in fig. 3.11.

3.3.7 Effect of EY concentration

Hydrogen generation rate increased sharply before 1:10 weight ratio of EY to Pt/ZnO and after that the increasing rate started to decrease. Therefore, EY concentration has a positive influence on hydrogen generation rate. As mentioned before, EY dye can absorb visible light and the electrons can transfer from the HOMO to the LUMO state, generating excited electrons and cationic radicals which is followed by electron-injection from dyes to Pt sites of the host photocatalyst.[37] However, EY dye needs to be absorbed on the photocatalyst surface to continue the above process.

The lower increasing rate of hydrogen generation can be attributed to dissociative EY dye molecules. Dissociative EY dye cannot perform electrons injection from dye molecules to Pt sites of the host photocatalysts. Moreover, it will absorb solar light which leads to light energy loss, resulting in the decreasing of hydrogen generation rate. Initially, the amount of EY dye that effectively got absorbed on photocatalyst increased with increasing EY concentration. There have been several studies confirmed that along with the increasing of EY dye concentration, gradual red shift phenomenon can be observed. It means the absorption of longer wavelength light was observed.[24,58] However, after the optimal point, dissociative EY dyes started to increase, leading to increasingly severe light energy loss.[24]

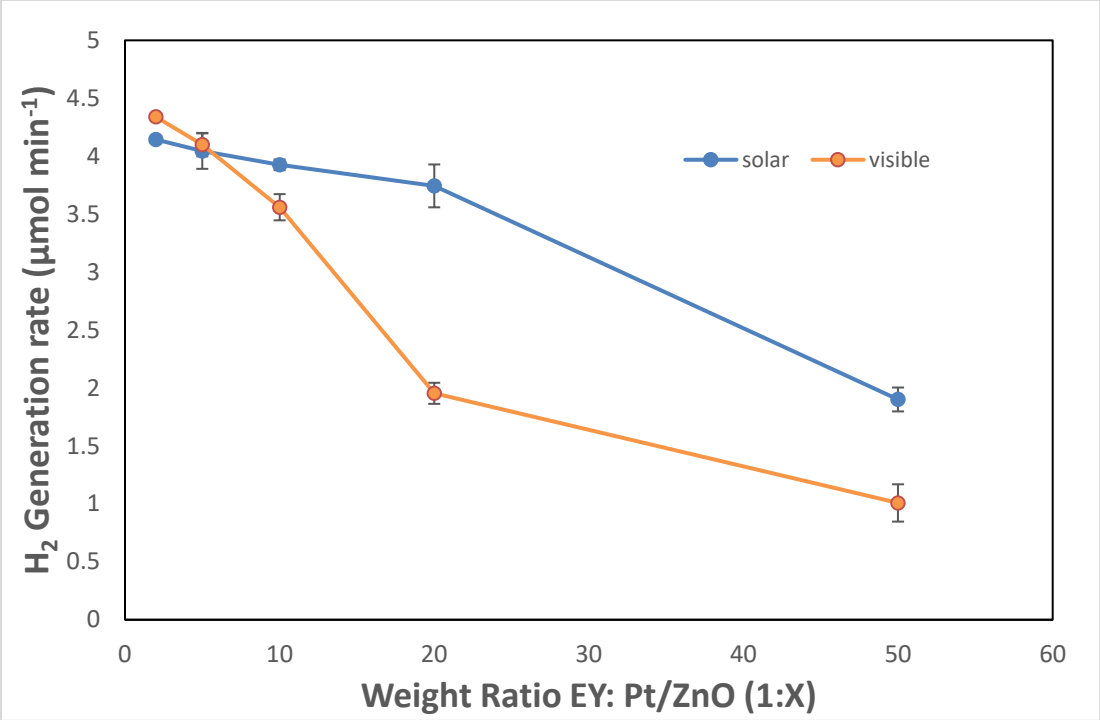

Figure 3.10 Dependence of weight ratio of EY to Pt/ZnO to hydrogen generation rate

3.3.8 Effect of photocatalyst loading

Concentration of photocatalyst Pt/ZnO is an important factor to hydrogen generation rate. While keeping dye concentration, TEOA concentration, pH value and solar intensity constant (10 v% TEOA, pH =7, 100 mW/cm^2 light intensity, 50 mg EY) constant, a series of experiments were conducted by varying the photocatalyst loading to investigate the effect of catalyst concentration to hydrogen generation rate. Hydrogen generation rate was found to increase linearly along with the increasing of catalyst concentration before 2.5 g/mol and then reached a plateau. The linear increasing pattern before 2.5 g/mol can be explained by the proportional increase of accessible active catalyst surface area with catalyst concentration. Therefore, the limiting factor of HER in this section can be concluded to be light absorbance and catalyst concentration. Turbidity is one of the main reasons that stops the continuous growth of hydrogen generation rate above the optimum point. High turbidity will exacerbate light scattering which leads to light energy loss.[59] Besides, aggregation and agglomeration caused by high photocatalyst concentration also

have negative effect on hydrogen generation rate for the loss of catalyst surface area.[60]

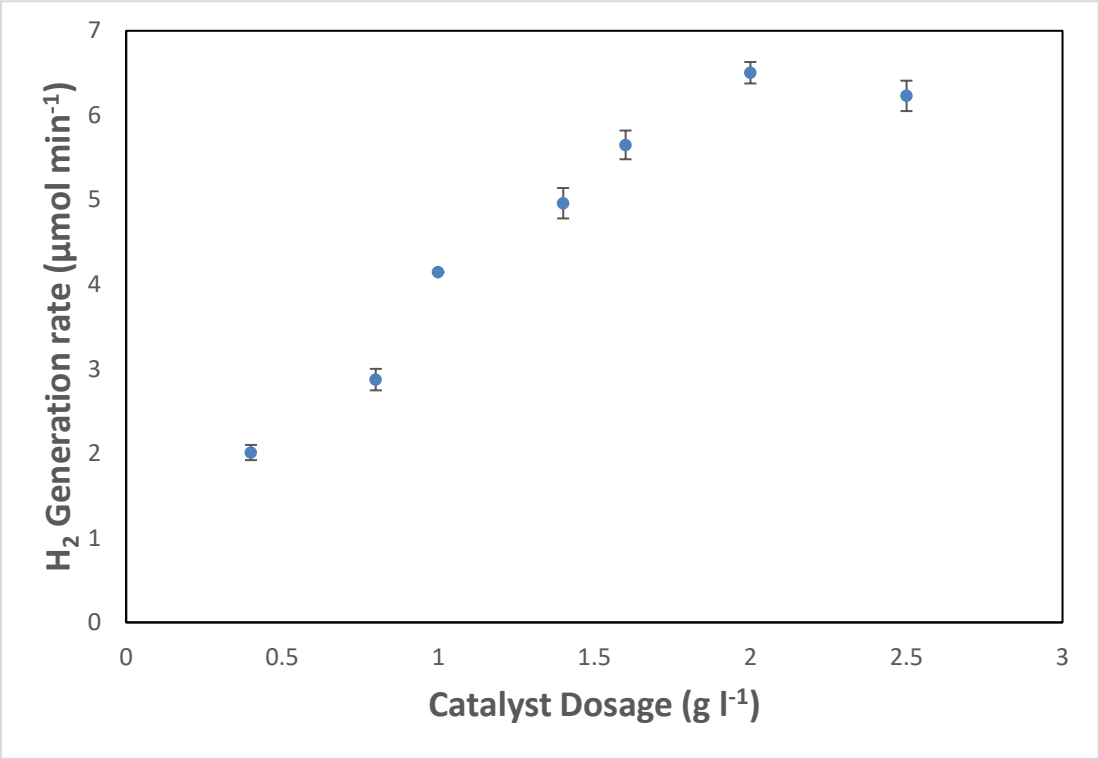

Figure 3. 1 1 **Dependence of catalyst dosage to hydrogen generation rate**

3.3.9 Regression analysis of experimental data

The regression analysis was applied to the experimental data by using Minitab software to relate H_2 generation rate as a response variable to a set of predictor variables including light intensity, EY content, pH, Pt content, and catalyst (Pt/ZnO) dosage. The H_2 generation rate data of experiments conducted under both visible and solar lights were combined. Normality of the data —the key assumption for the statistical analysis of experimental data — was confirmed by analyzing normal probability plots of the residuals[29]. The experimental data was clustered into three groups depending on the patterns of temporal variation of variables. The first group includes data describing the effect of light intensity and catalyst dosage on H_2 generation rate that has approximately linear dependence (Fig. 3.13), second and third groups describing the data of the effect of EY content, pH, and Pt content on H_2 generation rate have nonlinear behaviours (Fig.

3.14, Fig. 3). The commonly used significance level (α-level) of 0.05 was a criterion for interpreting the significance of calculated statistical estimates[61].

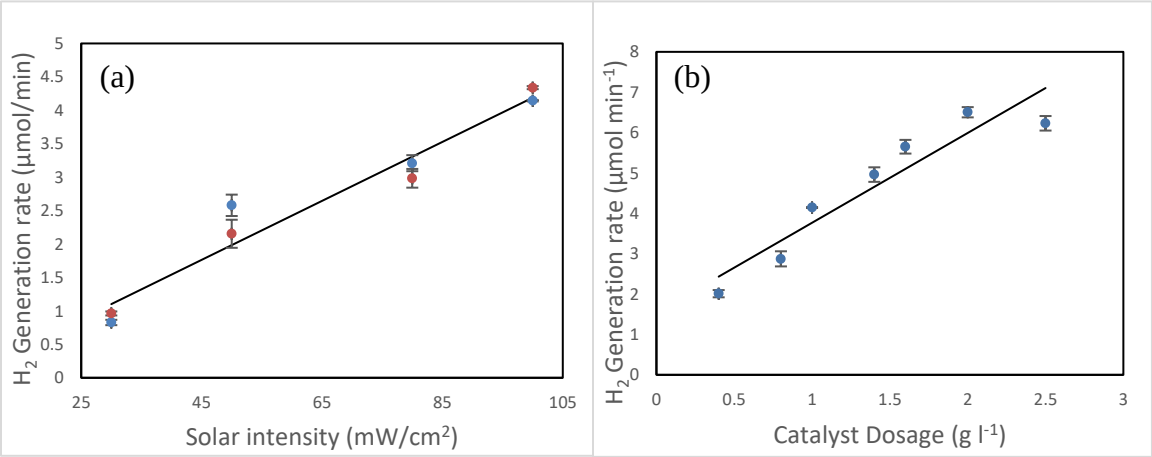

Figure 3. 1 2 **Group 1 fitted line of (a) solar intensity (b) catalyst dosage to hydrogen generation rate**

The first group was investigated by linear regression analysis. The data examination has been done with the application of analysis of variance (ANOVA) method[61]. The coefficients of determination R^2 giving the proportion of H_2 generation rate explained by the light intensity and catalyst dosage are 95% and 89% respectively. The numerical results of ANOVA are statistically significant in accordance with their corresponding p-values (≤0.05) and the linear regression models can be given as follows:

$$H_2 = -0.221 + 0.044 \cdot I \quad (16)$$

$$H_2 = 1.543 + 2.224 \cdot [C] \quad (17)$$

where H_2 – hydrogen generation rate μmol·min^{-1}, I – light intensity mW·cm^2, C – catalyst (Pt/ZnO) dosage g·l^{-1}. The Pearson correlation coefficients r to the models Eq. 16 and Eq. 17 are 0.97 and 0.94 respectively that fall within a strong correlation range.

The pH and Pt loading dependencies were approximated by nonlinear regression models:

$$H_2 = -6.661 \cdot Pt^2 + 12.110 \cdot Pt - 1.292 \quad (18)$$

$$H_2 = -0.678 \cdot pH^2 + 9.749 \cdot pH - 31.515 \quad (19)$$

where Pt – platinum content weight%

The calculated R^2 are 94% and 84% respectively. In nonlinear regression analysis the standard error of regression S is a more meaningful estimate of the goodness-of-fit rather than R^2. The calculated S values showing the average distance of the data points from the fitted lines described by Eq. 18, Eq. 19 are 0.38 and 0.82 μmol·min^{-1} respectively.

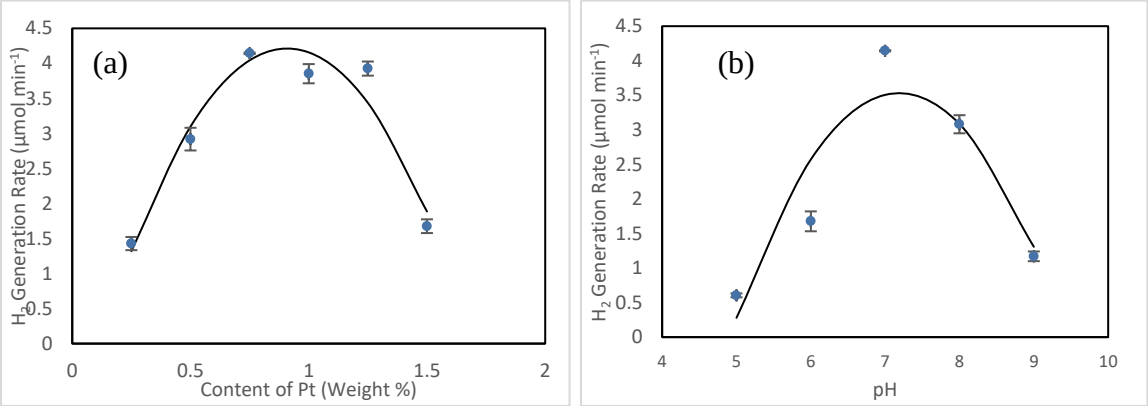

Figure 3. 1 **3 Fitted line of (a) content of Pt and (b) pH to hydrogen generation rate**

The last group of laboratory results of H_2 generation rate as functions of EY was approximated by the following nonlinear regression models:

$$H_2 = 4.178 - 4.324/(2 \text{ ^ } ([EY] / 0.030)) \quad (20)$$

where EY – Eosin Y content g l^{-1}.

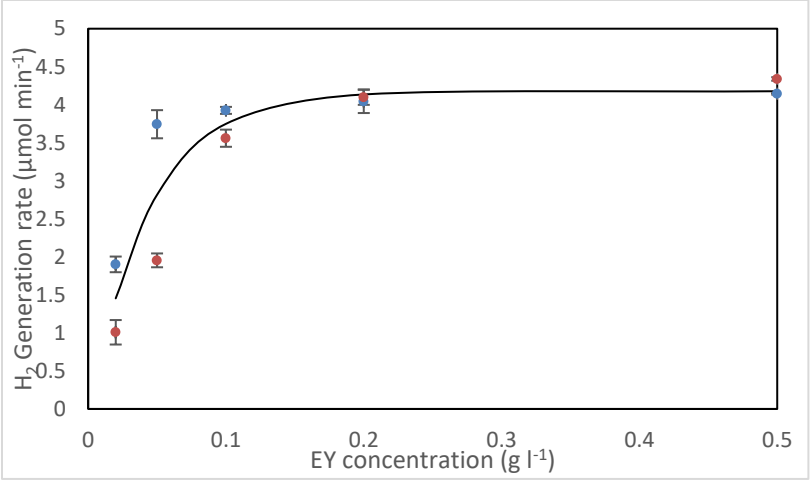

Figure 3. 1 4 **Fitted line of EY concentration to hydrogen generation rate**

The R^2 to the models above is 83% and the calculated S values is 0.55 µmol·min^{-1}. The p-

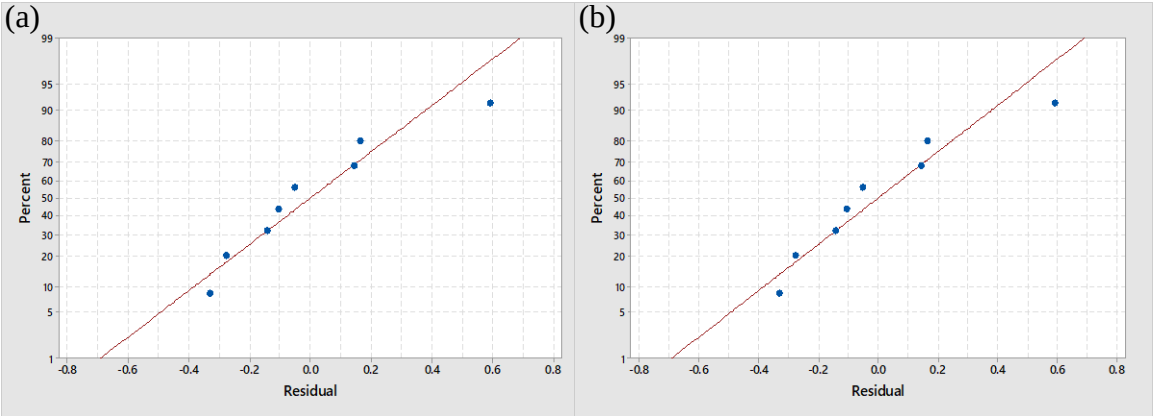

Figure 3. 1 5 **Normal probability plots of the residuals for H_2 generation rate where a) light intensity b) TEOA concentration are predictor variables**

values corresponding to the lack-of-fit test are greater than α-level concluding that the models (Eq. 20) accurately fit the experimental data. Calculations revealed the statistical significance of the models (Eq.16-20) that can be further used to predict the H_2 generation rate by varying the values of predictor variables – light intensity, TEOA concentration, EY content, pH, Pt content and catalyst (Pt/ZnO) dosage. The normality assumption is satisfied for all developed mathematical models as the analysis of normal probability plots of the residuals showed. An example of normal probability plots of the residuals for both linear and nonlinear regression models is presented in Fig. 3.16.

3.4 Conclusions

Platinum loading, TEOA concentration, EY concentration, solar intensity and pH value all play important roles in photocatalytic activities. The optimal point for platinum loading to ZnO is 0.75 w%. Neutral pH value (7.0) is the optimal condition for HER to happen. Light intensity has a positive effect on HER and solar and visible light didn't exert a huge difference on hydrogen generation rate under the same light intensity. TEOA concentration has a positive effect on photocatalytic activities of Pt/ZnO while the relation between TEOA concentration and Hydrogen generation rate fits well with Langmuir-Hinshelwood kinetic model. Before weight ratio of EY concentration to Pt/ZnO reached 1:10, it can effectively promote HER. Excessive loading of EY can increase turbidity and light energy loss and hereby no longer contributed to hydrogen generation rate. The highest hydrogen generation rate reached 6.504 μmol min^{-1} with 2.0 g l^{-1} of catalyst loading and after that the hydrogen generation rate starts decreasing because of the increasing turbidity and aggregation. This study has proved that Pt/ZnO have efficient photocatalytic activity for hydrogen generation and shed some light in the field of ZnO as host photocatalyst for hydrogen generation.

3.5 References:

1. Oceanic, N. & Holloway, R. Global atmospheric methane : budget , changes. 2058–2072 (2011). doi:10.1098/rsta.2010.0341

2. Hughes, L. Biological consequences of global warming: is the signal already apparent? *Trends Ecol. Evol.* **15,** 56–61 (2000).

3. Züttel, A., Borgschulte, A., Schlapbach, L. (Louis) & Wiley InterScience (Online service). *Hydrogen as a future energy carrier*. (Wiley-VCH, 2008).

4. Xu, J. & Froment, G. F. Methane steam reforming, methanation and water-gas shift: I. Intrinsic kinetics. *AIChE J.* **35,** 88–96 (1989).

5. Momirlan, M. & Veziroglu, T. N. The properties of hydrogen as fuel tomorrow in sustainable energy system for a cleaner planet. **30,** 795–802 (2005).

6. Haryanto, A., Fernando, S., Murali, N. & Adhikari, S. Current Status of Hydrogen Production Techniques by Steam Reforming of Ethanol: A Review. *Energy & Fuels* **19,** 2098–2106 (2005).

7. Fujishima, A. & Honda, K. Electrochemical photolysis of water at a semiconductor electrode. *Nature* **238,** 37–38 (1972).

8. Serpone*, N. Is the Band Gap of Pristine TiO2 Narrowed by Anion- and Cation-Doping of Titanium Dioxide in Second-Generation Photocatalysts? (2006). doi:10.1021/JP065659R

9. Wu, T., Lin, T., Zhao, J., Hidaka, H. & Serpone, N. TiO_2 -Assisted Photodegradation of Dyes. 9. Photooxidation of a Squarylium Cyanine Dye in Aqueous Dispersions under Visible Light Irradiation. *Environ. Sci. Technol.* **33,** 1379–1387 (1999).

10. Li, Z., Luo, W., Zhang, M., Feng, J. & Zou, Z. Environmental Science Photoelectrochemical cells for solar hydrogen production : current state of

promising photoelectrodes ,. 347–370 (2013). doi:10.1039/c2ee22618a

11. Sivula, K., Formal, F. Le & Grätzel, M. Solar Water Splitting : Progress Using Hematite (a -Fe 2 O 3) Photoelectrodes. 432–449 (2011). doi:10.1002/cssc.201000416

12. Liu, X., Wang, F. & Wang, Q. water splitting. 7894–7911 (2012). doi:10.1039/c2cp40976c

13. Martin, D. J. *et al.* Angewandte Highly Efficient Photocatalytic H 2 Evolution from Water using Visible Light and Structure-Controlled Graphitic Carbon Nitride **. 9240–9245 (2014). doi:10.1002/anie.201403375

14. Savio J. A. Moniz, S. A. S. Visible-light driven heterojunction photocatalysts for water splitting – a critical review. (2015). doi:10.1039/C4EE03271C

15. Editors, G., Nocera, D. & Guldi, D. 2009 Renewable Energy issue energy research. (2009). doi:10.1039/b800489g

16. Pelaez, M., Nolan, N., Pillai, S., … M. S.-A. C. B. & 2012, undefined. A review on the visible light active titanium dioxide photocatalysts for environmental applications. *Elsevier*

17. Chen, X., Shen, S., Guo, L. & Mao, S. S. Semiconductor-based photocatalytic hydrogen generation. *Chem. Rev.* **110,** 6503–6570 (2010).

18. Li, X. *et al.* Engineering heterogeneous semiconductors for solar water splitting. *J. Mater. Chem. A* **3,** 2485–2534 (2015).

19. Dai, K., Peng, T., Ke, D. & Wei, B. Photocatalytic hydrogen generation using a nanocomposite of multi-walled carbon nanotubes and TiO2 nanoparticles under visible light irradiation. *Nanotechnology* **20,** (2009).

20. Youngblood, W. J., Lee, S. A., Maeda, K. & Mallouk, T. E. Visible Light Water Splitting Using Dye- Sensitized Oxide Semiconductors. *Acc. Chem. Res.* **42,**

1966–1973 (2009).

21. Kamat, P. V. & Fox, M. A. Photosensitization of TiO2 colloids by Erythrosin B in acetonitrile. *Chem. Phys. Lett.* **102,** 379–384 (1983).

22. Xu, J., Li, Y. & Peng, S. Photocatalytic hydrogen evolution over Erythrosin B-sensitized graphitic carbon nitride with in situ grown molybdenum sulfide cocatalyst. *Int. J. Hydrogen Energy* **40,** 353–362 (2015).

23. Li, Q. *et al.* High-efficient photocatalytic hydrogen evolution on eosin Y-sensitized Ti− MCM41 zeolite under visible-light irradiation. *ACS Publ.*

24. Wang, L., Zhao, H., Chen, Y., Sun, R. & Han, B. Efficient photocatalytic hydrogen production from water over Pt – Eosin Y catalyst : A systemic study of reaction parameters. *Opt. Commun.* **370,** 122–126 (2016).

25. Chowdhury, P., Gomaa, H. & Ray, A. K. Chemosphere Sacrificial hydrogen generation from aqueous triethanolamine with Eosin Y-sensitized Pt / TiO 2 photocatalyst in UV , visible and solar light irradiation. **121,** 54–61 (2015).

26. Ehret, A., Stuhl, L. & Spitler, M. . Variation of carboxylate-functionalized cyanine dyes to produce efficient spectral sensitization of nanocrystalline solar cells. *Electrochim. Acta* **45,** 4553–4557 (2000).

27. Guo, M. *et al.* Photoelectrochemical studies of nanocrystalline TiO2 co-sensitized by novel cyanine dyes. *Sol. Energy Mater. Sol. Cells* **88,** 23–35 (2005).

28. Peng, T. *et al.* Photosensitization of different ruthenium(II) complex dyes on TiO2 for photocatalytic H2 evolution under visible-light. *Chem. Phys. Lett.* **460,** 216–219 (2008).

29. Chowdhury, P., Gomaa, H. & Ray, A. K. Factorial design analysis for dye-sensitized hydrogen generation from water. *Int. J. Hydrogen Energy* **36,** 13442–13451 (2011).

30. Liu, Y., Wei, S. & Gao, W. Ag/ZnO heterostructures and their photocatalytic activity under visible light: Effect of reducing medium. *J. Hazard. Mater.* **287,** 59–68 (2015).

31. Gomathisankar, P., Hachisuka, K., … H. K.-I. journal of & 2013, undefined. Enhanced photocatalytic hydrogen production from aqueous methanol solution using ZnO with simultaneous photodeposition of Cu. *Elsevier*

32. Ishii, T., Kato, H., A, A. K.-J. of P. and P. & 2004, undefined. H2 evolution from an aqueous methanol solution on SrTiO3 photocatalysts codoped with chromium and tantalum ions under visible light irradiation. *Elsevier*

33. Ahmad, H., Kamarudin, S. K., Minggu, L. J. & Kassim, M. Hydrogen from photo-catalytic water splitting process: A review. *Renew. Sustain. Energy Rev.* **43,** 599–610 (2015).

34. Bard, A. J. & Fox, M. A. Photosynthesis : Solar Splitting of Water to Hydrogen and Oxygen. 141–145 (1995). doi:10.1021/ar00051a007

35. Reza Gholipour, M., Dinh, C.-T., Béland, F. & Do, T.-O. Nanocomposite heterojunctions as sunlight-driven photocatalysts for hydrogen production from water splitting. *Nanoscale* **7,** 8187–8208 (2015).

36. Everly, C. R. & Traynham, J. G. Heterogeneous Photocatalytic Preparation of Supported Catalysts. Photodeposition of Platinum on Ti02 Powder and Other Substrates. 4317–4318 (1978).

37. Malekshoar, G. & Ray, A. K. In-situ grown molybdenum sul fi de on TiO 2 for dye-sensitized solar photocatalytic hydrogen generation. **152,** 35–44 (2016).

38. Yu, C. & Kai, Y. Novel hollow Pt-ZnO nanocomposite microposheres with hierarchical structure and enhanced photocatalytic activity and stability. 2142–2151 (2013). doi:10.1039/c2nr33595f

39. Zhang, M., Chen, C., Ma, W. & Zhao, J. Visible-Light-Induced Aerobic Oxidation

of Alcohols in a Coupled Photocatalytic System of Dye-Sensitized TiO_2 and TEMPO. *Angew. Chemie* **120,** 9876–9879 (2008).

40. Hannappel, T., Burfeindt, B., Storck, W., Mpg, F. Der & Willig, F. Measurement of Ultrafast Photoinduced Electron Transfer from Chemically Anchored Ru-Dye Molecules into Empty Electronic States in a Colloidal Anatase TiO 2 Film. **5647,** 6799–6802 (1997).

41. Ni, M., Leung, M. K. H., Leung, D. Y. C. & Sumathy, K. A review and recent developments in photocatalytic water-splitting using TiO2for hydrogen production. *Renew. Sustain. Energy Rev.* **11,** 401–425 (2007).

42. Majek, M., Filace, F. & Wangelin, A. J. Von. On the mechanism of photocatalytic reactions with eosin Y. 981–989 (2014). doi:10.3762/bjoc.10.97

43. Uchihara, T., Matsumura, M., Yamamoto, A. & Tsubomura, H. Effect of Platinum Loading an the Photocatalytic Activity and Luminescence of Cadmium Sulfide Powder. *J . Phys. Chem* **93,** 5870–5874 (1989).

44. Jiao, Y., Jiang, H. & Chen, F. RuO_2 /TiO_2 /Pt Ternary Photocatalysts with Epitaxial Heterojunction and Their Application in CO Oxidation. *ACS Catal.* **4,** 2249–2257 (2014).

45. Daneshvar, N., Aber, S., Seyed Dorraji, M. S., Khataee, A. R. & Rasoulifard, M. H. Photocatalytic degradation of the insecticide diazinon in the presence of prepared nanocrystalline ZnO powders under irradiation of UV-C light. *Sep. Purif. Technol.* **58,** 91–98 (2007).

46. Sakthivel, S. *et al.* Solar photocatalytic degradation of azo dye : comparison of photocatalytic efficiency of ZnO and TiO 2. **77,** 65–82 (2003).

47. Fouad, O. A., Ismail, A. A., Zaki, Z. I. & Mohamed, R. M. Zinc oxide thin films prepared by thermal evaporation deposition and its photocatalytic activity. *Appl. Catal. B Environ.* **62,** 144–149 (2006).

48. Moser, J. & Gratzel, M. Photosensitized Electron Injection in Colloidal Semiconductors. 6557–6564 (1984). doi:10.1021/ja00334a017

49. Lazarides, T. *et al.* Making Hydrogen from Water Using a Homogeneous System Without Noble Metals. **9,** 9192–9194 (2009).

50. Fu, H., Xu, T., Zhu, S. & Zhu, Y. Photocorrosion Inhibition and Enhancement of Photocatalytic Activity for ZnO via Hybridization with C $_{60}$. *Environ. Sci. Technol.* **42,** 8064–8069 (2008).

51. Rudd, A. L. & Breslin, C. B. Photo-induced dissolution of zinc in alkaline solutions. *Electrochim. Acta* **45,** 1571–1579 (2000).

52. Genscher, H. Electrochemical Behavior of Semiconductors under Illumination. *J. Electrochem. Soc.* **113,** 1174 (1966).

53. Pellegrin, Y. & Odobel, F. Sacrificial electron donor reagents for solar fuel production. *Comptes Rendus Chim.* **20,** 283–295 (2017).

54. Yang, X., Chen, B., Zheng, L., Wu, L. & Tung, C. hydrogenation of functionalized nitrobenzenes †. 1082–1086 (2014). doi:10.1039/c3gc42042f

55. Kumar, K. V., Porkodi, K. & Selvaganapathi, A. Constrain in solving Langmuir e Hinshelwood kinetic expression for the photocatalytic degradation of Auramine O aqueous solutions by ZnO catalyst. **75,** 246–249 (2007).

56. Senthilkumaar, S., Porkodi, K., Gomathi, R., Maheswari, A. G. & Manonmani, N. Sol e gel derived silver doped nanocrystalline titania catalysed photodegradation of methylene blue from aqueous solution. **69,** 22–30 (2006).

57. Poulios, I., Micropoulou, E., Panou, R. & Kostopoulou, E. Photooxidation of eosin Y in the presence of semiconducting oxides. **41,** 345–355 (2003).

58. Xu, J., Li, Y., Peng, S., Lu, G. & Li, S. Eosin Y-sensitized graphitic carbon nitride fabricated by heating urea for visible light photocatalytic hydrogen evolution: the

effect of the pyrolysis temperature of urea. 7657–7665 (2013). doi:10.1039/c3cp44687e

59. Chowdhury, P., Malekshoar, G., Ray, M. B., Zhu, J. & Ray, A. K. Sacrificial Hydrogen Generation from Formaldehyde with Pt / TiO 2 Photocatalyst in Solar Radiation. (2013).

60. Park, S.-J. *et al.* Crucial factors for catalyst aggregation and deactivation on Co/Al2O3 in a slurry-phase Fischer–Tropsch synthesis. *Appl. Catal. A Gen.* **413–414,** 310–321 (2012).

61. Chatterjee, S. & Hadi, A. S. *Regression analysis by example*.

4 Conclusions and recommendations

This thesis has investigated the potential of EY-sensitized Pt/ZnO on hydrogen production under solar and visible light irradiation. Six parameters were studied on their effect to hydrogen generation rate, which are Pt loading content, light intensity, pH value, TEOA concentration, EY concentration and photocatalyst loading. All of them have positive effect on the photocatalytic activity of Pt/ZnO before their optimal point and regression analysis was conducted on each parameter for prediction of hydrogen generation rate when other parameters were kept in optimal situations. The results showed that 0.75w% Pt/ZnO exhibited highest activity with hydrogen generation rate of 6.504 μmol min^{-1} under solar light irradiation.

For further studies of this system, recommendations are listed below:

- Since Pt/ZnO nanoparticles have been proved to have efficient photocatalytic activities for hydrogen generation, morphology studies can be followed up to further enhance the photocatalytic activity of Pt/ZnO, such as core-shell model or multi-layer model.
- Since batch reactor was used in experimental section, the structure of reactor can be improved based on the face that hydrogen has the tendency to gather at the top of the reactor for its small density. If the reactor can have better circulation, the results will be more accurate.
- The stability of the system need to be further enhanced for the hydrogen generation rate will decrease along with ongoing of experiment.

Curriculum Vitae

Name:	Tianfang Tian
Post-secondary Education and Degrees:	Dalian University of Technology Dalian, Liaoning, China 2012-2016 B.E. The University of Western Ontario London, Ontario, Canada 2016-2018 MESc.
Honours and Awards:	Mitacs Globalink Fellowship 2016-2017,
Related Work Experience	Teaching Assistant The University of Western Ontario 2016-2018